2002

Infrared, Raman and surface-enhanced resonance Raman scattering of N-butylimido, ethyleneamine perylene (PTCD-NH(2)): Single-molecule detection using colloidal silver and silver island films.

Tibebe. Lemma Mukria
University of Windsor

INFRARED, RAMAN AND SURFACE-ENHANCED RESONANCE RAMAN SCATTERING OF N-BUTYLIMIDO, ETHYLENEAMINE PERYLENE (PTCD-NH_2). SINGLE MOLECULE DETECTION USING COLLOIDAL SILVER AND SILVER ISLAND FILMS

BY

TIBEBE LEMMA MUKRIA

A Thesis

Submitted to the Faculty of Graduate Studies and Research through the School of Physical Sciences in partial fulfilment of the requirement for the Degree of Master of Science at

The University of Windsor.

Windsor, Ontario, Canada
2002

ABSTRACT

The vibrational spectra and the surface-enhanced (resonance) Raman scattering (SERS/SERRS) of a perylene dye containing a terminal NH_2 group, n-butylimido, ethyleneamine perylene (PTCD-NH_2) have been studied. The infrared, Raman and resonance Raman spectra of the material were recorded and vibrational fundamentals assigned. The vibrational assignments of fundamentals were aided with an *ab-Initio* Hartree-Folk at 6-31G level of theory. Langmuir-Blodgett monolayers of the neat material were fabricated and the π-A isotherms recorded. Mixed monolayers were also studied for applications in SERRS. The spectra of evaporated thin solid films were obtained and a complete spectroscopic characterization of these films is presented in the thesis.

Single molecule detection of PTCD-NH_2, adsorbed on colloidal silver and silver island films are investigated using surface enhanced resonance Raman spectroscopy and Langmuir-Blodgett films. Single molecules detection (SMD) is achieved by dilution of the analyte and added to colloidal silver. Analyte concentration ranges from 10^{-4} to 10^{-12}M and also by vacuum evaporating a silver overlayer onto a Langmuir-Blodgett (LB) monolayer containing 1, 10 and 100 target molecules per micron square of surface area. In resonance Raman scattering (RRS) and SERRS the dominant bands are those of perylene chromophore. The LB technique is ideally suited to obtain spatially resolved spectra of single dye molecules dispersed in the matrix of a fatty acid, and it is used here to obtain SERRS from dye molecules found within the area of illumination. SERRS spectra were also obtained from silver sols placed on polysilane-coated quartz, and from germanium slides. A laser line of 514.5 nm was used for SERRS measurements. For the SERS measurements the 633 nm and 780 nm laser lines were used for excitation. The characteristic fundamental vibrational frequencies observed in the single molecule SERRS spectra are unequivocally assigned with the help of their first overtones and combinations.

DEDICATION

I would like to dedicate this thesis to the memory of my brother, Wondesen Lemma and to my family and friends.

ACKNOWLEDGEMENT

I would like to take this opportunity to thank my mentor Dr. Aroca for his incredible and tireless supervision and direction.

The past and present members of Materials and Surface Science Group: Dr. Carlos, Dr. Patricia, Dr. Alicia, Teo, Nick, Paul, Ben and Daniel. I would also thank all the secretaries and staff of the Physical Science department at the University of Windsor, especially Pat Aroca.
My thanks are also extended to Dr. Rumfeldt.

TABLE OF CONTENTS

List of Figures

List of Tables

List of Abbreviations

AFM: Atomic Force Microscopy

SEVS: Surface Enhanced Vibrational Spectroscopy

RRS: Resonance Raman Spectroscopy

SERS: Surface Enhanced Raman Spectroscopy

SERRS: Surface Enhanced Resonance Raman Spectroscopy

SEF: Surface Enhanced Fluorescence

SMS: Single Molecule Spectroscopy

SMD: Single Molecule Detection

RAIRS: Reflection Absorption Infrared Spectroscopy

LB: Langmuir- Blodgett

UHV: Ultra High Vacuum

OTS: Octadecyltrichlorosilane

PTCD-NH_2: N-(n-butyl)-N'-(2-aminoethyl) Perylene-3,4,9,10-Tetracarboxylic Acid Diimide

μ_i = Electric dipole

α_{ij} = Molecular polar izability

INTRODUCTION

1. The Vibrational Spectra of perylene tetracarboxylic derivatives

1.1. Vibrational Spectroscopy

The study of molecular vibrations leads to the theory of infrared and Raman spectra[1-3]. The basic theory of vibrational spectroscopy applies to gases, liquids and has extended include crystalline and non-crystalline matter[2]. Vibrational spectroscopy is the most powerful analytical tool for dealing with the identification, interactions, fabrication or manipulation of molecules in the gas, liquid or solid state. The apparent simplicity of vibrational analysis comes from the success of classical models of masses hanging from a uniform spring which allows one to relate the spring constant to chemical bond's force constant, and its periodic oscillations to stretching vibrations of chemical bonds. In fact, a simple classical formula permits to calculate the force constant given the vibrational wavenumber ω in cm^{-1} and the reduced mass μ (g) of the oscillating chemical bond:

$$k\ (mdyn\ Å^{-1}) = 5.891829 \times 10^{-7}\ \mu\omega^2 \qquad (1)$$

The latter is one of the most commonly used analytical tools by chemists and biochemists in their quest for identification of functional groups in molecules. Twenty years after the discovery of SERS,[4,5] the theory of molecular vibrations has been extended further to include the special chapter of adsorbed molecules on surfaces and interfaces. The new surface-enhanced vibrational spectroscopy (SEVS) is the study of molecular vibrations of adsorbates on surfaces and interfaces that can enhance the absorption or the emission of electromagnetic radiation. In parallel with the classical theory of molecular vibrations, SEVS comprises the theory of surface-enhanced infrared and surface-enhanced Raman scattering. SEVS is a branch of the more general field of Surface Enhanced Spectroscopy (SES), a very active area of basic research with a broad range of analytical applications.

The vibrational spectra of perylene tetracarboxylic derivatives (PTCDs) have been studied by several groups. However, the SEVS spectra of PTCDs have been almost exclusively studied in our group. Although the PTCDs are macrocycles with more that 150 fundamental normal modes of vibration, the discussion of their vibrational spectrum can be reduced to a few characteristic vibrational modes that serve as probes for analytical characterization and applications to molecular organisation studies, molecule-metal surface interactions and single molecule studies. In practise, the assignment of observed vibrational bands is reduced to the fundamental vibrations of the chromophore PTCD. The latter is particularly true in the case of resonance Raman scattering (RRS). The local symmetry of the chromophore (planar moiety) allows the separation of normal modes according to the direction of their dynamic dipoles, helping the assignment of infrared active vibrations. For molecular orientation determination the most relevant normal modes are the in-plane carbonyl stretching vibrations, ring stretching vibrations and the out-of-plane C-H wagging modes. The term out-of-plane is used here to indicate the local planar structure of the chromophore. Similarly, a number of intense infrared bands that can be assigned to "in-plane" C-H bending modes and ring stretching vibrations in the 1000-1450 cm^{-1} spectral region. The assignment of characteristic vibrational wavenumbers observed in the infrared and Raman spectra are helped by the computed wavenumbers and intensities as will be shown for PTCD-NH_2 . Vibrational assignments are obtained using the animation of the atomic displacements given by the solution of the vibrational problem in Gaussian. Clearly, quantum computations are now an essential part of the most common analytical tools used for materials characterization.

1.2. Single Molecule Spectroscopy

Single molecule spectroscopy (SMS) [6-13] is a new technique which can be used to monitor interaction and reaction of an individual molecule with its environment. Unlike the detection of an ensemble of molecules which only yields an average values, detection of an individual molecule reveals the full distribution

of molecular parameters. The size of the effective cross section is a key factor for single molecule spectroscopy, since the effective cross section must be large enough to generate a detectable spectroscopic signal from a single molecule. From single molecule fluorescence experiments it is known that effective cross sections for optical single molecule detection should be on the order of 10^{-16}–10^{-17}cm^2 per molecule[14-16]. Molecules with low (small cross section), fluorescence signal need to be labeled with a special marker such as "dye" in order to achieve high enough fluorescence cross sections. For inelastic scattering (Raman) enhancing the optical signal is essential for developing a single molecule spectroscopy. Surface enhanced Raman scattering (SERS) with enhancement factors as high as 15 orders of magnitudes[6,7,10,11,17-20], could provide effective Raman cross sections (10^{-16} cm^2) at the same level of effective fluorescence cross sections. It has been demonstrated that SERS[21] could be an effective method for detection of a single molecule.

SERS active substrates, which provide a large enhancement factor, are the most important requirement for single molecule SERS spectroscopy. Silver, gold and also copper have been prepared in a variety of ways to generate SERS active substrate for various applications. Colloidal silver or gold particles, and in particular their aggregates have been shown to give very high SERS enhancement factor.[9,22,23] For single molecule detection in solution, small silver and gold colloidal clusters with sizes between about 100 and 1000 nm are very useful SERS-active substrates. Target molecules are physically adsorbed or chemically attached to these nanostructures or metallic particles. In the very close vicinity of such structures, local optical fields can be strongly enhanced when collective excitation of conduction electrons, called surface plasmon resonance are excited. Unique high field enhancement seems to exist in so-called "hot spots"[7,17,24] of clusters, formed by silver and gold nanoparticles or island films of these metals.

1.3. Surface – Enhanced Resonance Raman Scattering

Since the first observation of the enhanced Raman signal of pyridine adsorbed on an electrochemically roughened silver electrode by Fleischmann *et al* [25]extensive experimental and theoretical investigation of the phenomenon have led to substantial progress in identifying possible mechanisms to explain the effect. Jeanmaire and Van duyne[26] and Albrecht and Creighton[27] independently proposed that the enormously strong Raman signal measured from pyridine on a rough silver electrode must be caused by surface enhancement of the Raman scattering. Thousands of SERS papers, have appeared to date and hence several excellent reviews have been contributed by Otto [28], Moskovits [20], Birke and Lombardi [29] Creighton [30], Pettinger[31], Campion and Kambhampati[32], Tuan Vo-Dinh[33], Kneipp and her co-workers[10], Aroca and Kovacs. [34] Detailed and some relatively conclusive descriptions of SERS models and mechanisms have been given in the latter reviews. In SERS two types of mechanisms are widely accepted. The electromagnetic enhancement effect (EME), which consider the change of the local electric field around the adsorbed molecules. The chemical enhancement (CE) mechanism primarily involves a charge transfer state between the surface complex of the adsorbed molecule and a metal surface. However, the electromagnetic effect is dominant, and the chemical effect contribute on to the enhancement is estimated to be a maximum of two orders of magnitude.[35] The electromagnetic enhancement (EME) is dependent on the presence of metal surface's roughness features, or metal nanostructure, while the chemical enhancement (CE) involves changes to the adsorbate electronic state due to chemisorption of the analyte.[36].

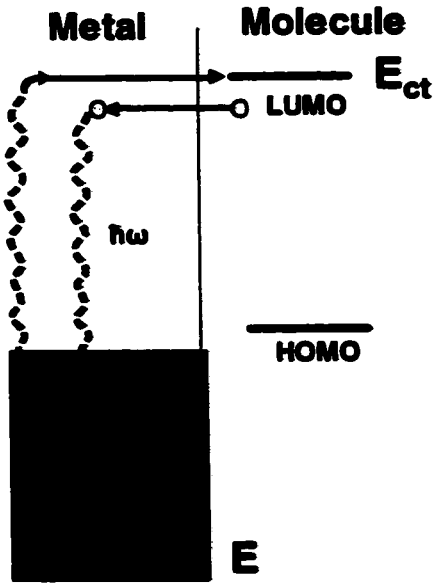

Figure 1: Schematic diagram of chemical effect.

The EM enhancement is primarily due to plasmon excitation in metal nanostructures, and the effect is mostly limited to a few metals for which surface plasmons can be excited by visible radiation, in particular Cu, Ag and Au. Theoretically, many metals would be capable of exhibiting SERS, but the coinage and alkali metals satisfy calculable requirements and provide the strongest enhancement in the visible. [20] Metals such as Pd or Pt exhibit enhancements of about 10^2-10^3 for excitation in the near infrared. [20]

The combination of surface- and resonance-enhancement (SERRS)[6,7,11] can occur when adsorbates have intense electronic absorption bands in the same spectral region as the metal surface plasmon resonance, yielding an overall enhancement as large as 10^{10} - 10^{15}.

The sensitivity of SERRS far exceeds that of any other technique, which is capable of providing structural information. A further advantage is that very often the intense luminescence background that sometimes results from laser excitation under resonance conditions is almost completely quenched in

SERRS. Resonance Raman techniques in the visible require no extra equipment.

1.4. Surface-Enhanced Resonance Raman Scattering of single molecule

The analytical applications of SERS, and particularly SERRS, for the detection of attomole quantities were realized very early in the development of surface-enhanced Raman scattering [25]. The concept of spatially resolved SERS/SERRS was discussed, as a technique key to achieving the detection of a few molecules in a solid matrix. The advent of single molecule SERS was discussed in the SERS literature in 1990. For instance K. Kneipp wrote [37] the "advantage of SERS, in particular for single molecule detection, results from the number of photons which can be scattered by one molecule". Single Molecule Spectroscopy (SMS) is now a growing field with an increasing number of practitioners[10,38]. We have recently reported [39] SERRS experiments carried out using Raman-microscopy with 1 μm^2 spatial resolution that permits one to achieve spatially resolved single molecule detection of dyes dispersed in a single monolayer fabricated with the Langmuir-Blodgett technique. The latter work takes advantage of the resonance Raman effect in addition to surface-enhancement provided by vacuum evaporated silver island films. In contrast, all previous single molecule SERS work has been carried out on single or aggregated colloidal metal particles[6,7,11,12]. Single molecule detection using surface-enhanced resonance Raman scattering (SERRS) is also achieved from dye molecules adsorbed on colloidal silver. The single molecule SERRS is accomplished using mixed Langmuir-Blodgett (LB) layers and silver overlayer of 6 nm mass thickness. A perylene tetracarboxylic (PTCD) dye molecule with a terminal NH_2 group has been synthesized to facilitate adsorption to silver surfaces. The PTCD-NH_2 molecule has an absorption band in full resonance with the 514.5 nm laser line used in the Raman experiments. Previous results have been obtained for other PTCD molecules which have shown no spectroscopic evidence of chemical adsorption onto silver surfaces. Here, the results of single-molecule SERRS, of the dye chemisorbed onto colloidal

particles in solution, are compared with the results of silver overlayers deposited onto a single LB monolayer containing 1 to 100 molecules of the dye per μm^2 of surface area.

The resonance Raman scattering (RRS) spectra of PTCD-NH_2 is well characterized by the observation and assignment of fundamentals, first, second and third overtones and combination bands of the most characteristic stretching modes of the aromatic perylene tetracarboxylic core.

Langmuir-Blodgett films of neat PTCD-NH_2 , and mixed LB films of PTCD-NH_2 and eicosanoic or arachidic acid $C_{19}H_{39}COOH$ (AA) were fabricated in a Lauda Langmuir film balance, which was cleaned with acetone and ultra pure water (18.2 MΩcm). Ultra pure water at 15°C, containing cadmium chloride (2.5 X 10^{-4} mol L^{-1}) was used as the subphase. After spreading the solution containing PTCD-NH_2 in AA, 20 minutes were allowed for evaporation of the solvent. Samples were fabricated at 15°C with a constant compression speed of 35 mm min^{-1}. The LB monolayer was transferred to Corning 7059 glass slides, quartz, and germanium substrates using an electronically controlled dipping device,Lauda Film Lift FL-1, and keeping a constant pressure of 24 mNm^{-1}. After waiting for the solid phase to stabilize, the substrate was lifted at 3 mm min^{-1} (Z-deposition). The transfer ratio was found to be approximately unity. Neat LB monolayers of PTCD-NH_2 and AA were also deposited onto glass substrates to be used as references. Resonance Raman Scattering (RRS) spectra were recorded using the neat PTCD-NH_2 LB monolayer on glass, and SERRS spectra were recorded using the LB monolayer deposited onto silver islands.

2. EXPERIMENTAL AND TECHNIQUES

2.1. Micro Raman Spectroscopy

Raman microscopy is now an established technique for probing the chemical and structural nature of a microscopic length scale. Despite the relatively weak absolute intensity from Raman scattering, Raman microscopy has become a routine analytical technique in recent years. This has been achieved by the use of highly efficient optical filtering and detection components, combined with a spectrometer that is optically matched to a microscope.[40] This type of instrument is readily adaptable to operate under confocal conditions, thus providing an improvement in the spatial discrimination and resolution.[41]

The Raman scattering, Raman resonance spectroscopy (RRS) and Surface-enhanced Raman resonance spectroscopy (SERRS) spectra were obtained using a Renishaw RM2000 (micro-Raman system) equipped with a computer controlled 3-axis encoded (XYZ) motorized stage, Figure 2. The RM2000 uses a Leica microscope (DMLM series) and is equipped with electrically cooled CCD array (-70°C). The spectrograph was equipped with a 1200 g/mm grating with additional angle-tuned bandpass filter optics. The laser beam was focused on the sample through the 50X and an oil immersion objectives (40X, 0.80NA) that also collected the scattered radiation (backscattering geometry). Raman spectra were recorded with ca. 4 cm^{-1} resolution using the 514.5 nm laser line of a Spectra-Physics argon ion laser (Lexel 95), 632.8 nm He-Ne laser line (Model 127) and the 780 nm diode laser line (Renishaw). For the 514 nm laser line, the power at the sample ranges from 0.8 mW (8.00 $X10^4 W/cm^2$) to 0.05 mW (5.00 $X\ 10^3\ W/cm^2$). For the measurement of LB monolayer and silver island films, the laser power was reduced to 0.05mW to avoid photodecomposition of the sample. To compensate for the reduced laser power, 20-40 scans were accumulated. Even at low power, decomposition could not be prevented completely, as evidence by the appearance of new bands. The instrument is equipped with 50XL and an oil immersion microscope objectives to focus the laser beam onto the surface of the monolayer film or to get signal from less than a nanoliter scattering volume from sample solutions. Confocality

can be used to increase the spatial resolution of the system. All spectra were acquired at room temperature. Data acquisition and analysis were carried out using the WIRE software for Windows and Galactic Industries GRAMS/32™ C software[42].

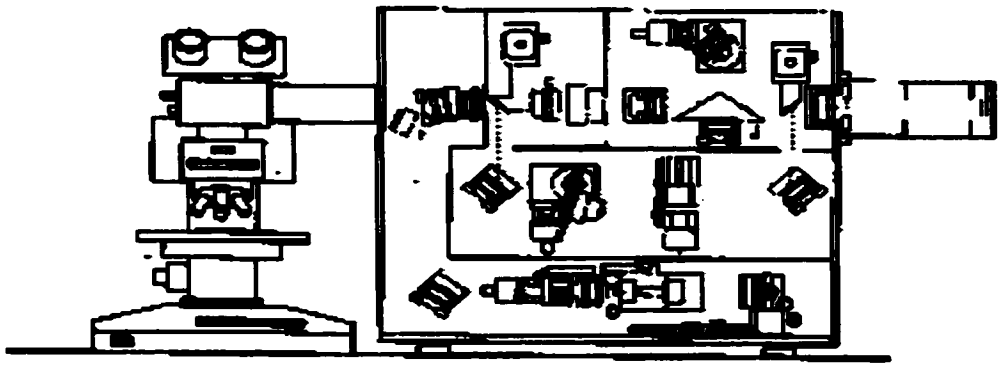

Figure 2: Illustration of the Renishaw Research Microscope Raman 2000 Instrument.

2.2. FT-IR and UV-Vis

The infrared spectra were recorded with the Bomem DA3 Fourier transform infrared Spectrophotometer equipped with a liquid nitrogen wide range MCT and DTGS detectors Figure 3.

The UV-Vis absorption spectra were routinely collected on the Varian 50 UV-VIS single beam spectroscopy Figure 4.

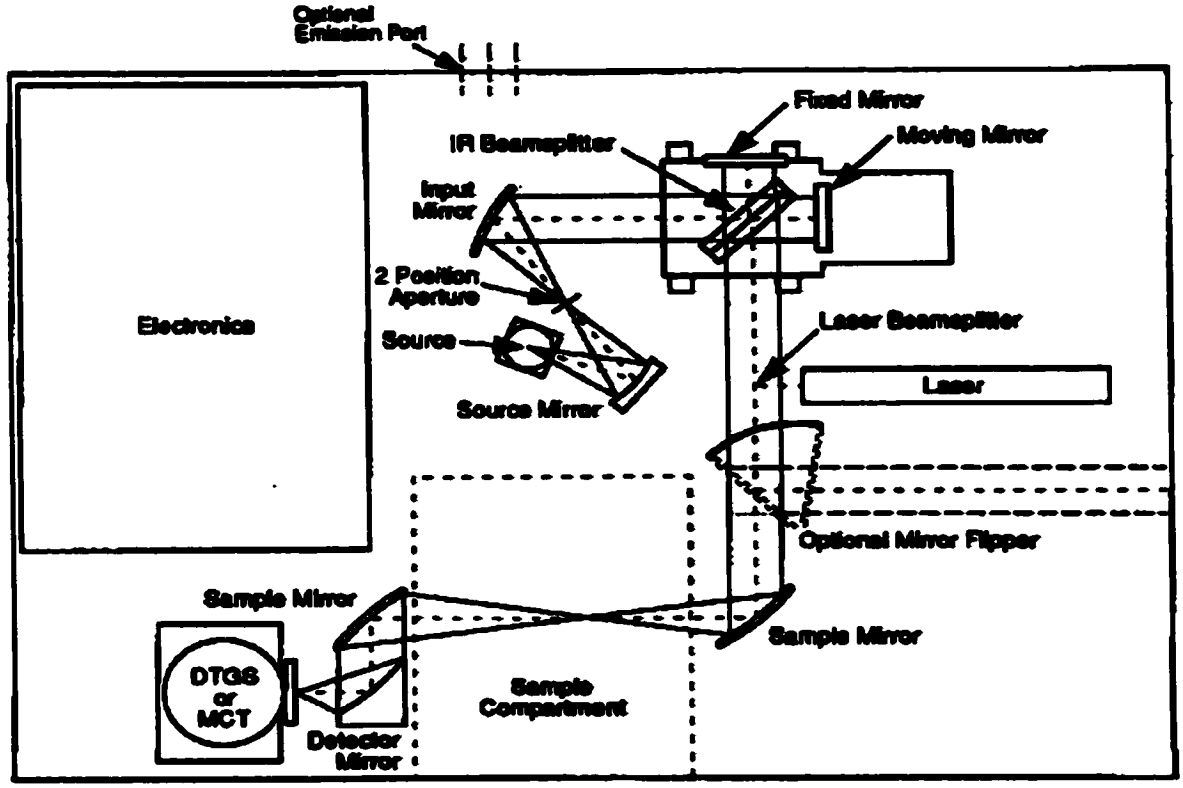

Figure 3: Optical configuration of Bomen DA3 FT-IR instrument.

This instrument is an example of a temporal dispersive instrument and operates via a sequential linear scan. It contains a continuous xenon lamp light source that flashes only when acquiring a data point thereby preventing degradation of photosensitive samples and allowing a collection rate of 80 data points per second. The wavelength selector consists of a monochrometer with a motor driven reflection-grating system that sweeps the spectral region of interest at a constant rate. A photoelectric detector enables detection of the radiant energy and the detection is synchronized with the motion of the grating allowing a wavelength scale based upon time to be recorded. A beam splitter is employed to enable simultaneous reference beam correction. The spectral range for this instrument is 190-1100 nm. Data acquisition is performed on the Cary WinUV software for windows, while data is manipulated using the Galactic Industries GRAMS/32 ™ C software.[42]

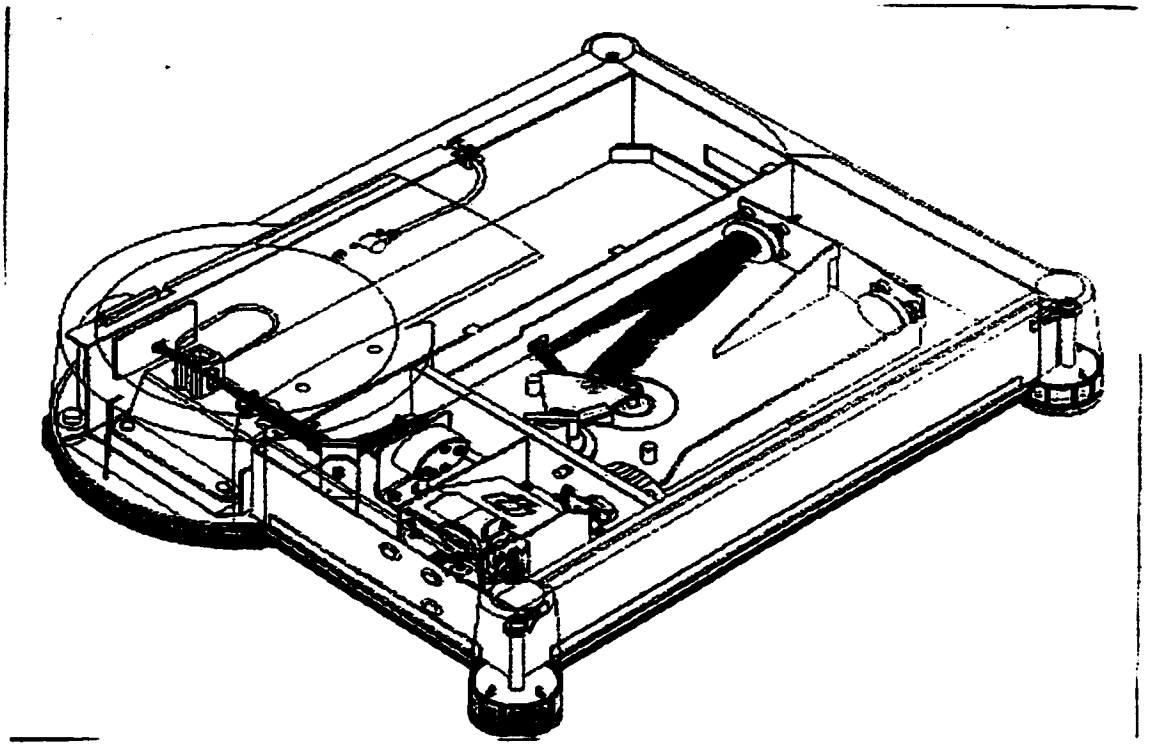

Figure 4 : Illustration of the Cary 50 UV-VIS spectrometer.

2.3. Vacuum Evaporation System

Metal films were prepared in a Balzers high vacuum system evaporator, equipped with an Edwards E2M2 rotary vacuum pump which functions as precursor to the Edwards diffusion pump as shown in Figure 5. Silver shot (Aldrich 20, 436-6) was evaporated thermally from a cupped tungsten boat using a Blazer BSV 080 glow discharge/evaporation unit. The pressure range was typically 10^{-6} mbar and was measured by Blazers IKR 020 cold cathode gauge. Silver was deposited to a total mass thickness of 6 nm at a rate of 0.5 Å s^{-1} onto a glass substrate preheated to 200°C. The deposition rate was allowed to stabilize before the shutter was opened. Film thickness and deposition rates were monitored using an XTC Inficon quartz crystal oscillator. The bulk density of silver employed was 10.5g cm^{-3}, the tooling factor 105%, and the Z-ratio, 0.529.

EVAPORATION SYSTEM

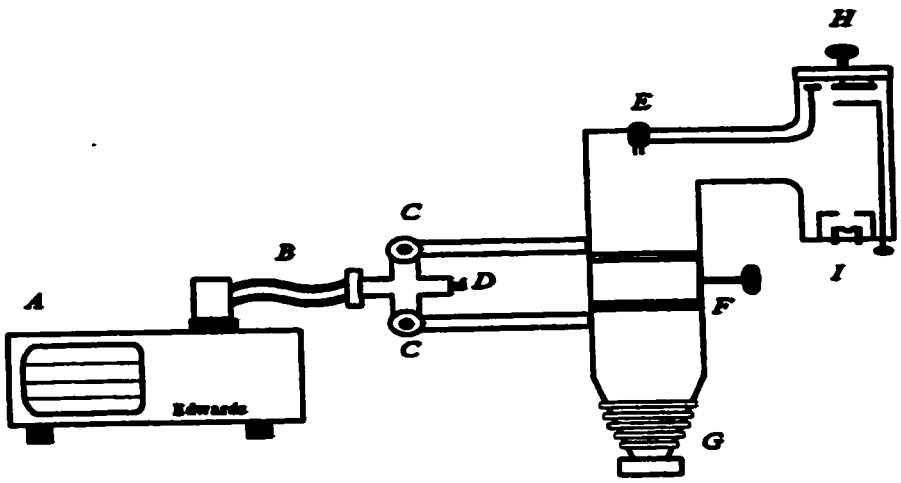

KEY:

A	FOREPUMP
B	HIGH VACUUM CONNECTOR HOSE
C	VALVES
D	PRESSURE RELEASE VALVE
E	INSTRUMENTATION FEEDTHROUGH: HIGH PRESSURE GAUGE, DEPOSITION RATE GAUGE
F	BUTTERFLY VALVE
G	DIFFUSION PUMP
H	LID: SUBSTRATE TABLE, THERMOCOUPLE AND HEATING ELEMENT FEEDTHROUGHS
I	BASE: THERMOEVAPORATION POSTS, SOURCE BOAT, CONTROL FOR SUBSTRATE SHIELD

Figure 5 : Evaporation system.

PTCD-NH_2 films of different thickness 6 and 10 nm were deposited onto continuous silver films (100 nm mass thickness) and silver island films (mass thickness of 6 nm) on a glass substrate. The perylene dye was evaporated from tantalum boats and the deposition rate was ~ 0.5Å s^{-1}. The bulk density used for the PTCD-NH_2 was 1g cm^{-3}, the tooling factor 92% and the Z-ratio was 0.1.

For visible absorption and fluorescence work, the substrates used were Corning 7059 glass slides. The glass slides had previously been cleaned by

deionized water and dipped into an acetone solution. For transmission FT-IR measurement a mass thickness of 30 nm PTCD-NH_2 evaporated on the KBr substrate. And for reflection absorption infrared spectroscopy, a mass thickness of 100 nm of silver and 100nm of PTCD-NH_2 powder were deposited on a glass substrates. Silver islands of 6 nm mass thickness, were used for surface-enhanced resonance Raman scattering (SERRS) experiments.

2.4. Langmuir- Blodgett Films

Langmuir-Blodgett monolayer films were prepared on a Lauda Langmuir film balance equipped with an electronically controlled dipping device lauda Filmlift FL-1 shown in Figure 6.

The Lauda trough and the barrier were thoroughly cleaned with deionized water, with a specific resistance of 18.2 MΩcm. The system was then cleaned with acetone. These steps were repeated at least three times before the system was finally flushed with deionized water and wiped dry with Kim wipes. The trough was then refilled with deionized water and the barrier calibrated. The monolayer forming materials were dissolved in a solution of 90% dichloromethane and 10 % spectroscopic grade trifluoroacetic acid from Aldrich. These solutions (10^{-3}-10^{-4} M) were then carefully spread in small droplets over the trough, via a micro syringe. Milli-Q purified water with a measured resistivity of 18.2 MΩcm containing cadmium chloride (2.5 X 10^{-4} mol L^{-1}) was used as the suphase. The spread solution was allowed to sit for approximately thirty minutes to evaporate the solvent. Once the solvent had evaporated, the film was compressed at 20 mm min^{-1} by a single barrier. An area of 150mm (trough width) X 187 mm (distance between the barrier and the pressure sensor) = 2.81 X 10^4 mm^2 was occupied by the Langmuir film at zero surface pressure. The average number of PTCD-NH_2 molecules confined per square micron on the subphase can be estimated by the product of the PTCD-NH_2 concentration in solution (1.44 X 10^{-10} mol L^{-1}) X Avogadro's number X volume of the solution spread (500 µL) divided by the area (area: 150 X 144= 2.16 X 10^4 mm^2) occupied by the Langmuir

film in its condensed phase in μm^2. Following the same procedure, LB monolayers were prepared containing on average one (300µL X 1.196 X 10^{-10}mol L^{-1} X 6.023 X 10^{23} molecules mol^{-1} / 2.16 X10^{10} μm^2 = 1), 7,10 100 PTCD-NH_2 molecules, dispersed in AA, per μm^2 of surface area.

The surface pressure-area isotherm of PTCD-NH_2 was recorded by compressing the trough area at 20 mm min^{-1}. The preparation of floating monolayers at the air-water interface was successful, and reproducible isotherms were recorded at 15°C where the area/molecule extrapolated to zero surface pressure was found to be 15 $Å^2$. LB films were transferred to a variety of substrate in order to explore the surface enhanced vibrational phenomena.

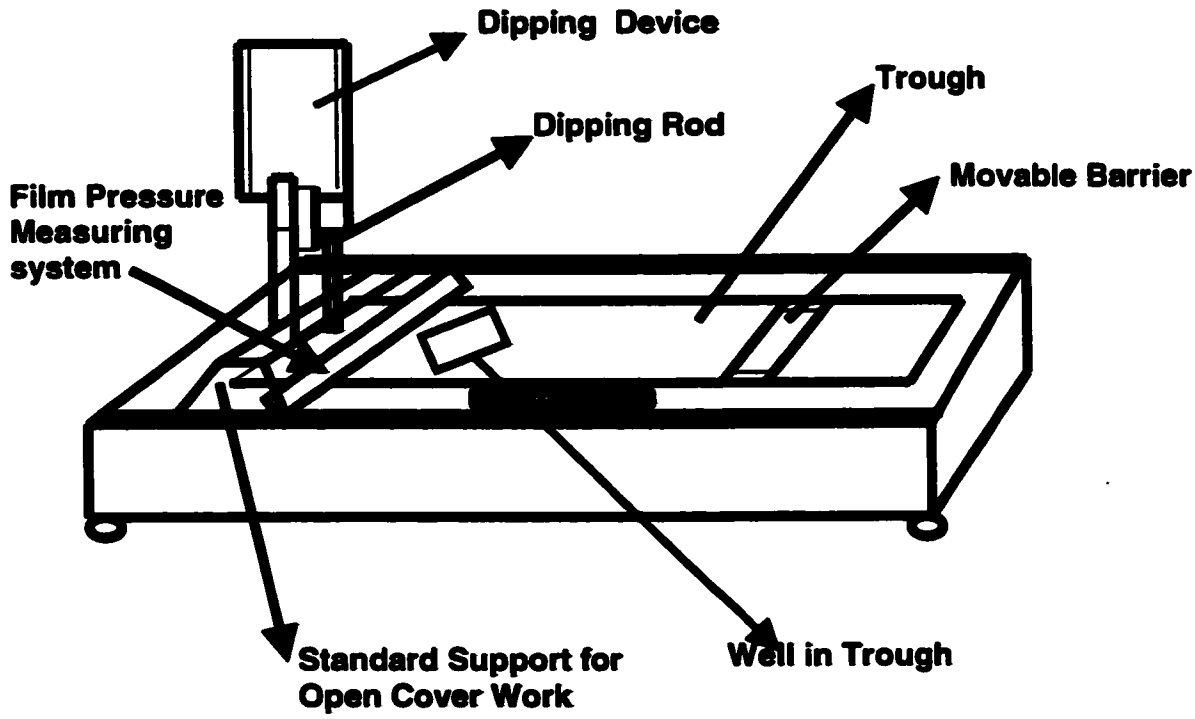

Figure 6: A schematic diagram of a Langmuir – Blodgett trough.

2.5. Colloid Preparation and Properties

Silver colloid is commonly used for SERS. It is possible to form monodispersed silver colloids by chemically reducing silver ions in solutions.[43,44]

Silver monoparticles can be rapidly produced by a strong reducing agents, such as borohydrate or sodium citrate. There is a long nucleation period, resulting in particles of varying sizes.[45] For example, the commonly used citrate reduction method[46], produces a distribution of particles different sizes and shapes [47]. These colloids give a good SERS enhancement [45]. It is also been reported that greater enhancement of Raman activity can be produced using particles of a narrowed size range.[48] The borohydride reduction method [49] can produce small particles that are fairly monodisperse but the reaction is not easy to control. [50] Nevertheless, both procedures provide reproducible results.

The colloid solutions used in this study were prepared according to the description of Lee and Meisel [51]. Sodium citrate, sodium borotetrahydride and octadecyltrichlorosilane were purchased from Aldrich. All the chemicals used were analytical grade and redistilled deionized water was used for the preparation of all the solutions. The first solution was prepared by the standard citrate reduction by dissolving 90 mg ($AgNO_3$) in 500 mL of H_2O and brought to boiling. A solution of 1% sodium citrate (10mL) was added. The solution then diluted with water in the ratio of 1:7. The absorption spectrum of this brownish solution has a maximum at 406 nm (Figure 8A). The second colloid was prepared by adding a solution of 1.00 X 10^{-3}M $AgNO_3$ (20 mL) portionwise to 60mL of vigorously stirred ice cold 2 X 10^{-3} $NaBH_4$. These yellowish Ag sols had absorption maxima at 400 nm (see Figure 7B). These colloidal suspensions were stable for several weeks and were stored in the dark.

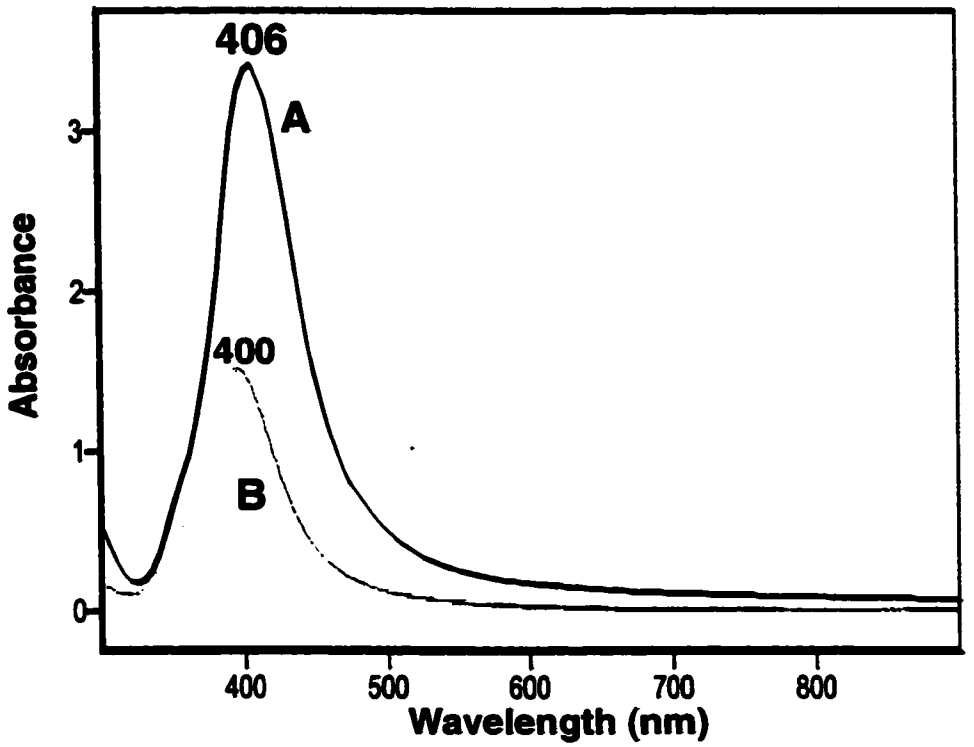

Figure 7: Extinction spectra of the colloidal silver solutions. (A) Citrate, (B) borohydride colloid solutions.

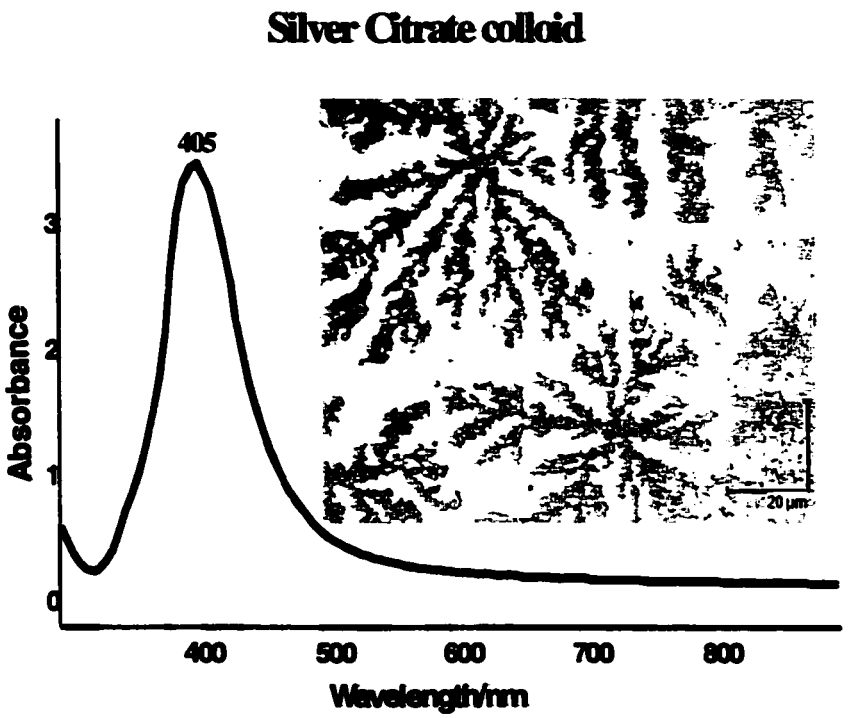

Figure 8: Absorption spectra of silver citrate solution, dried on freshly cleaved mica, imaged in air.

Polysilane Preparation: Polysilane solution was prepared by diluting 39 µL of Octadecyltrichlorosilane with 99.96 mL of toluene. The final concentration was approximately 10^{-3} M.

2.6 Atomic Force Microscopy (AFM) of Colloids.

AFM images were obtained by measurement of the force on a sharp tip created by the proximity to the surface of the sample.[52] This force is kept small and at a constant level with a feedback mechanism. When the tip is moved sideways it will follow the surface morphology.

AFM of colloid images were performed by Bill Price at the Department of Chemistry, Wayne State University, Detroit Michigan, USA.

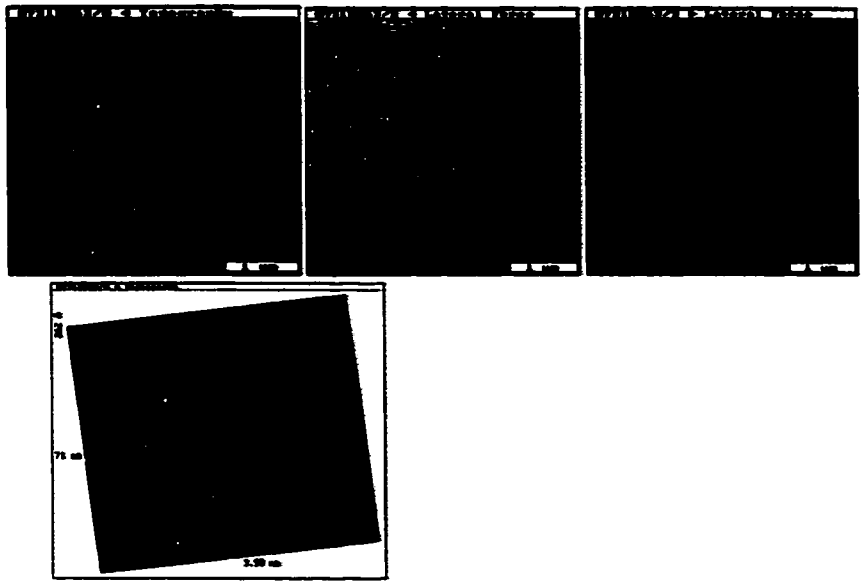

Figure 9: AFM topographic and lateral force images of the silver nanoparticles.

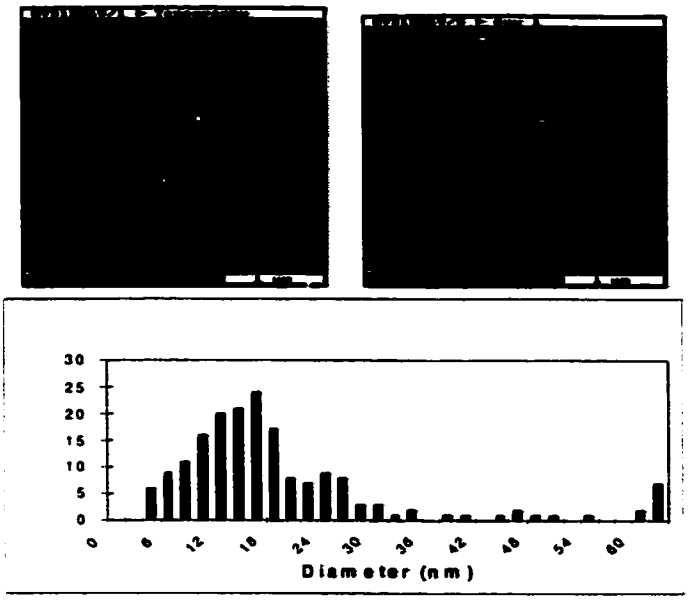

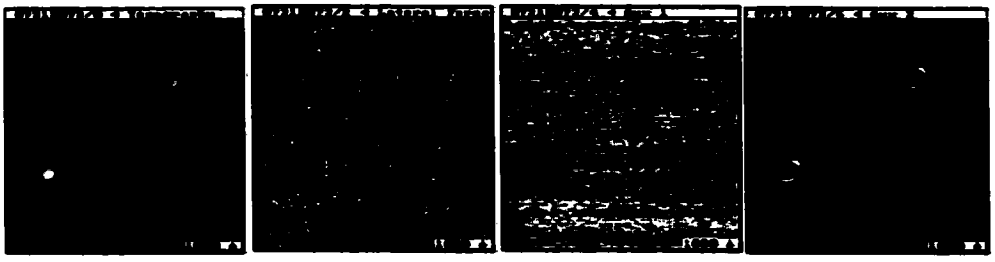

Figure 10: AFM topographic and lateral force images of the distribution and isolated silver nanoparticles.

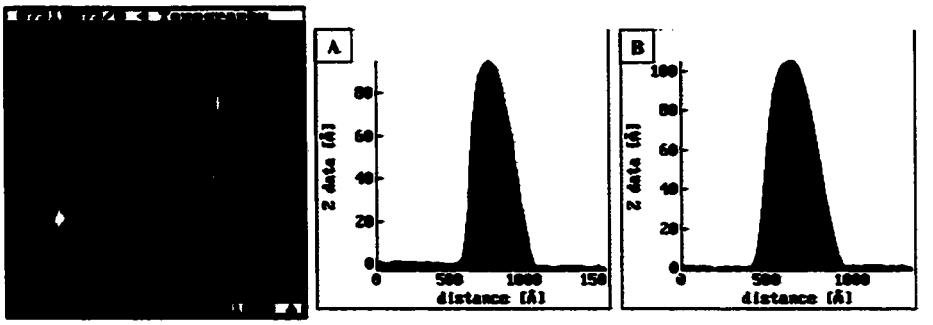

Figure 11: AFM topographic and lateral force images of the silver isolated nanoparticles.

3. SPECTROSCOPY CHARACTERIZATION OF PTCD-NH_2

3.1 Electronic Spectra

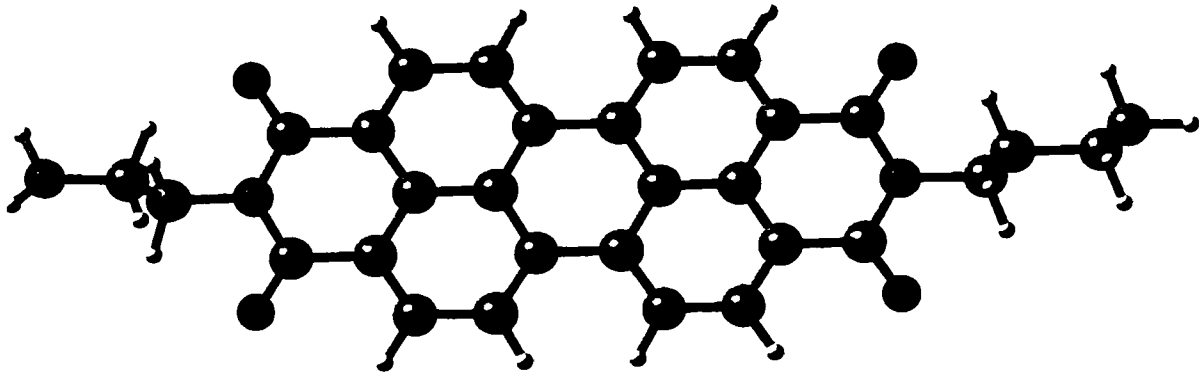

Figure 12: HF/6-31G optimized molecular structure of PTCD-NH_2

The equilibrium geometry of PTCDNH_2 presents a planar chromophore as shown in Figure 12, and it is this chromophore that gives the PTCDs their characteristic electronic spectra. The observed electronic absorption spectra of perylene tetracarboxylic derivatives containing one or two perylene chromophores usually consists of one electronic transition[53-55] with the corresponding vibronic structure as shown in Figure 13 for PTCD-NH_2. This characteristic vibronic structure associated with the π-π^* transition of the perylene moiety presents a 0-0 band at 541 nm followed by subsequent vibronic transitions at 504 and 473 nm. The molar absorptivity at 541 nm is 1.75×10^4 L mol^{-1} cm^{-1}. And the cross section is calculated to be 2.91×10^{-17} cm^2 $molecule^{-1}$.

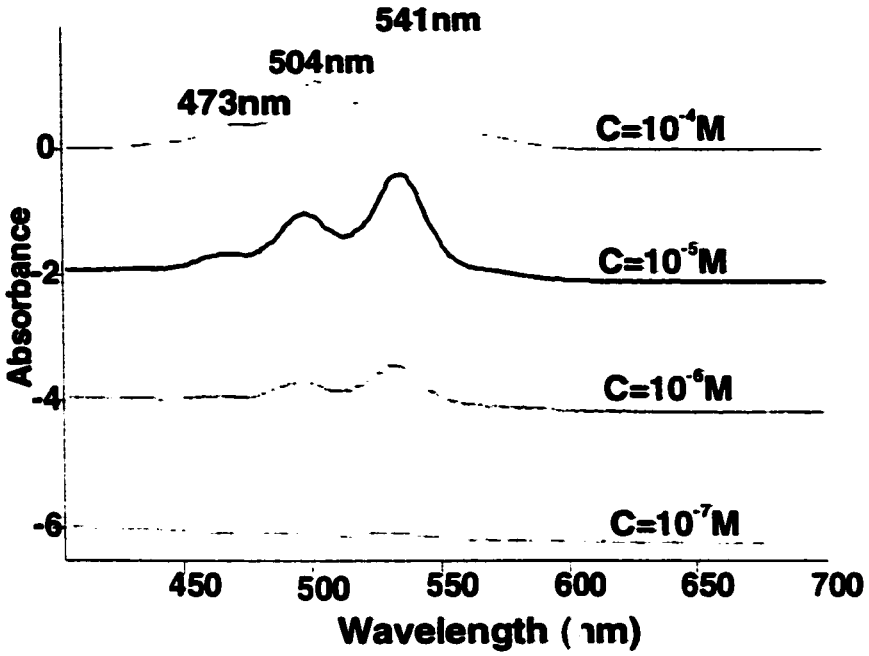

Figure 13: Absorption spectra of PTCD-NH_2 in CH_2Cl_2 solution.

The absorption spectrum of one LB monolayer is shown in Figure 14. Maximum was observed at 470 and 560 nm for PTCD-NH_2. Measured spectra in solution, in a KBr solid matrix and in an LB film are illustrated in Figure 16 for PTCD-NH_2. The electronic spectrum of the LB sample is broadened, and presented a red-shifted band with respect to 0-0 band of monomers in solution. Kahsa *et al.* have shown that the formation of dimers could result in hypsochromic or bathochromic shifts in the monomer band depending on the geometry of transitional dipoles in the composite molecule. [56] In this study, it confirmed the formation of dimers in the LB film.

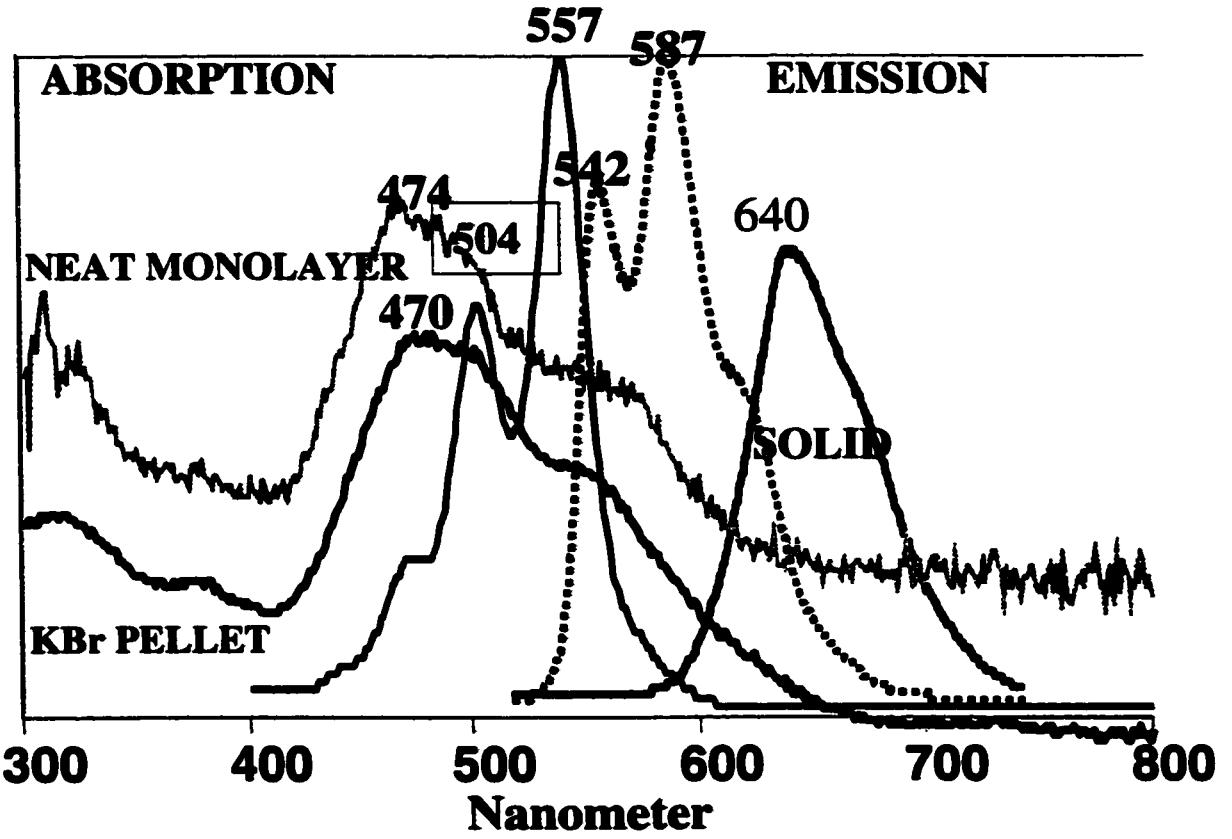

Figure 14: Absorption and emission spectra of PTCD-NH_2 solution in CH_2Cl_2 and solid samples: PTCD-NH_2 solid dispersed in a KBr pellet, neat monolayer on glass. Fluorescence was obtained with excitation wavelength at 514.5 nm.

The emission spectra of dichloromethane solutions of the PTCD-NH_2 were measured at different concentrations using a 514.5 nm excitation line. Figure 15 Measured spectra in solution, in a KBr solid matrix and in an LB film are illustrated in Figure 16 for PTCD-NH_2. The fluorescence spectra of the same solutions yield a mirror image of the absorption spectrum with maxima at 563,

603 nm and a weaker band at 655 nm. Each of the dilute solution spectra showed the three typical fluorescence bands associated with the monomer fluorescence of condensed aromatics.

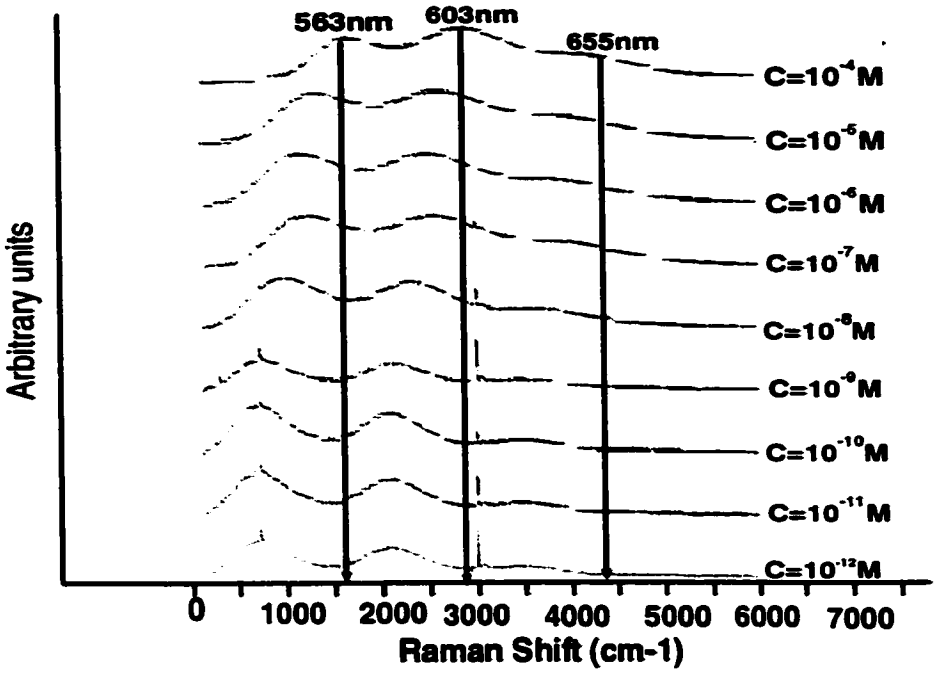

Figure 15: Fluorescence spectra of diluted PTCD-NH_2 in CH_2Cl_2 solution.

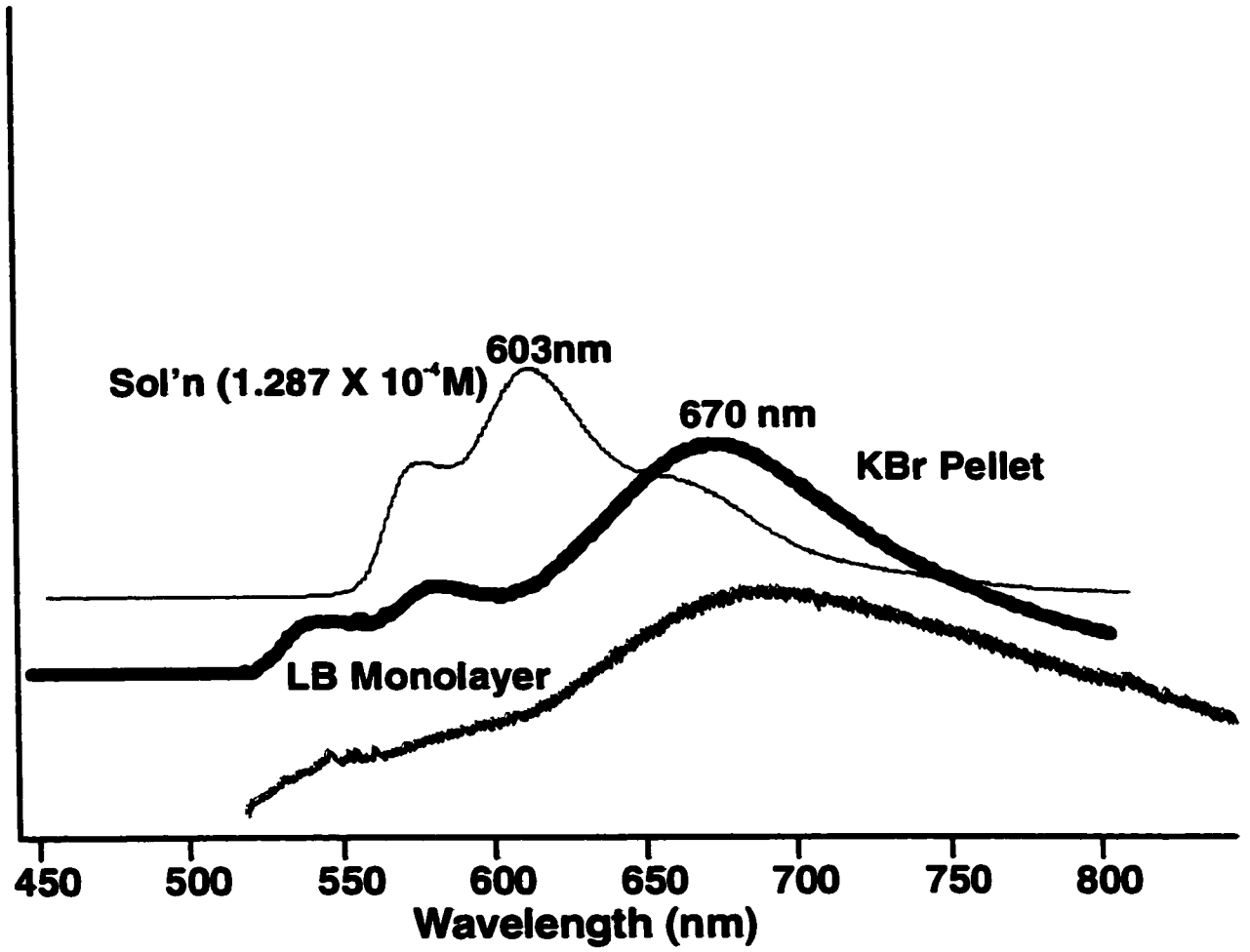

Figure 16: Fluorescence spectra of PTCD-NH_2 in CH_2Cl_2, in a KBr pellet and of one LB monolayer.

The absorption and emission spectra of the solid state, as LB films or dispersed in KBr pellets, are quite different from the solution spectra and, for comparison, they are shown in Figure 16. The absorption of the KBr pellet shows the main bands centered at 560, 504 and 474 nm, whereas the emission has a broad peak at 640 nm [2,4] This broad, structureless, red-shifted emission was clearly identified as the excimer emission Figure 14.[57] The formation of aggregates in the ground state and excimers in the excited state depends on the spatial arrangement of the aromatic rings.[22]

3.2. Surface- Enhanced Fluorescence (SEF)

The fluorescence of a dye molecule near a surface of a silver island film exhibits a maximum enhancement of the apparent quantum yield at a certain distance away from the surface.[58,59] Using a simple spherical model, the electromagnetic mechanism predicts that the distance dependence of the enhancement changes as $(r/r+d)^{12}$ for a molecule located at a distance d from a silver sphere of radius r. At the same time, for the competing energy transfer to the metal, the loss rate decreases as $1/d^3$ with absolute distance of molecule surface separation, [60] i.e., the energy transfer or damping is a faster decaying function of the molecule metal separation. A plot of these two functions in Figure 17 (r= 100 Å and d changing from 1 to 30 Å) showing that EM enhancement has a maximum at a certain distance. At that distance the EM enhancement overcomes the quenching, and enhanced emission is observed.

The excimer emission at 640 nm obtained with a 514.5 nm laser line for LB on silver and on glass, is shown in Figure 15. The observation of very strong excimer emission is due to the formation of organized structures or molecular stacking in LB films, which requires the chromophores to arrange with parallel and overlapping ring systems, as has been observed in α- perylene crystals. [61] The excimer emission of the monolayer on silver is enhanced in comparison with the LB film on glass (Figure 16). Using integrated intensities, an enhancement factor of 10 is obtained for SEF of the excimer emission.

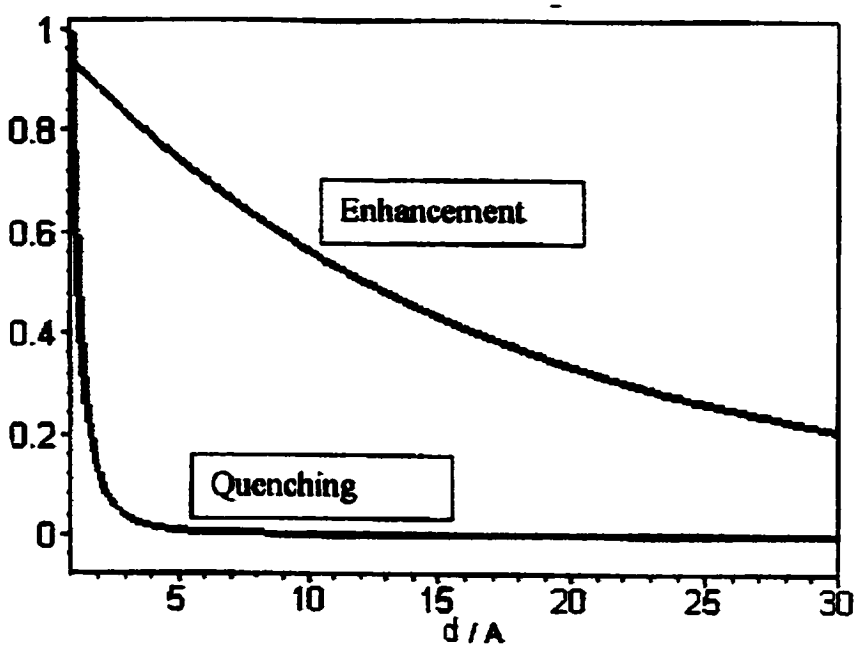

Figure 17: Theoretical calculation for dependence of EM enhancement (red) and quenching (green) of fluorescence on the distance between one molecule and the surface of a metallic sphere.

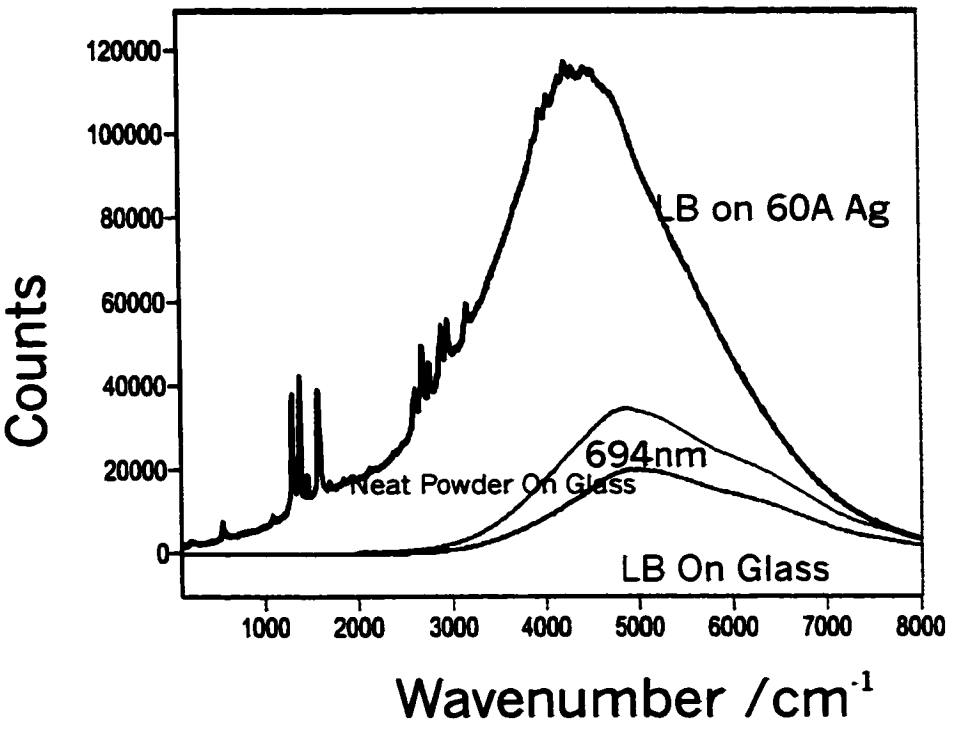

Figure 18: Fluorescence spectra for LB monolayer film of PTCD-NH_2 on both silver islands and glass using 514.5 nm laser line.

3.3. Molecular Vibrations: Infrared and Raman spectra

The molecular structure of PTCD-NH_2 is shown in Figure 12. The molecule belongs to the C_1 symmetry group and all vibrational fundamentals are allowed in the infrared and Raman spectra. There are (3x60-6) = 174 vibrational modes including 66 stretching and 108 bending vibrations. Assuming that the chromophore is planar, there are locally 73 in-plane modes and 38 out-of-plane modes. The vibrational assignment of PTCD-NH_2 was helped using *ab initio* theoretical computations of frequencies and intensities. There are a limited number of bands which could readily be assigned. The functional group NH_2 which is responsible for the chemical adsorption of the molecule attached as a

lateral chain. Even though this group has not a significant effect on either Raman or Infrared activities, it plays a significant role in the chemistry of the surface silver particle. The observed wavenumbers in the Raman and infrared spectra of PTCD-NH_2, their relative intensities and the calculated vibrational spectrum are listed in Table 1 and 2.(Page 36 and 44)

3.3.1. Calculated Spectra

The theoretical calculation were performed using Hartree-Fock (HF)[62,63] with a 6-31G basis set, to help the assignment of the vibrational Raman and Infrared spectra of PTCD-NH_2. Since HF calculations do not take electron correlation into consideration, predicted wavenumber values have to be scaled with a general scaling factor (0.9) to adjust observed experimental wavenumber values. The HF calculations were carried out using GAUSSIAN 98[42] software for Windows. The calculated geometry is presented in Table I and the computed dipole moments are μ_x= 0.02, μ_y= 0.10, μ_z= 0.40 Debye) and the polarizability are (α_{xx}= 604, α_{xy}= 0.579, α_{xz}= 347, α_{yy}= 11.05, α_{zy}= 1.065, α_{zz}= 130.6$C^2m^2J^{-1}$).

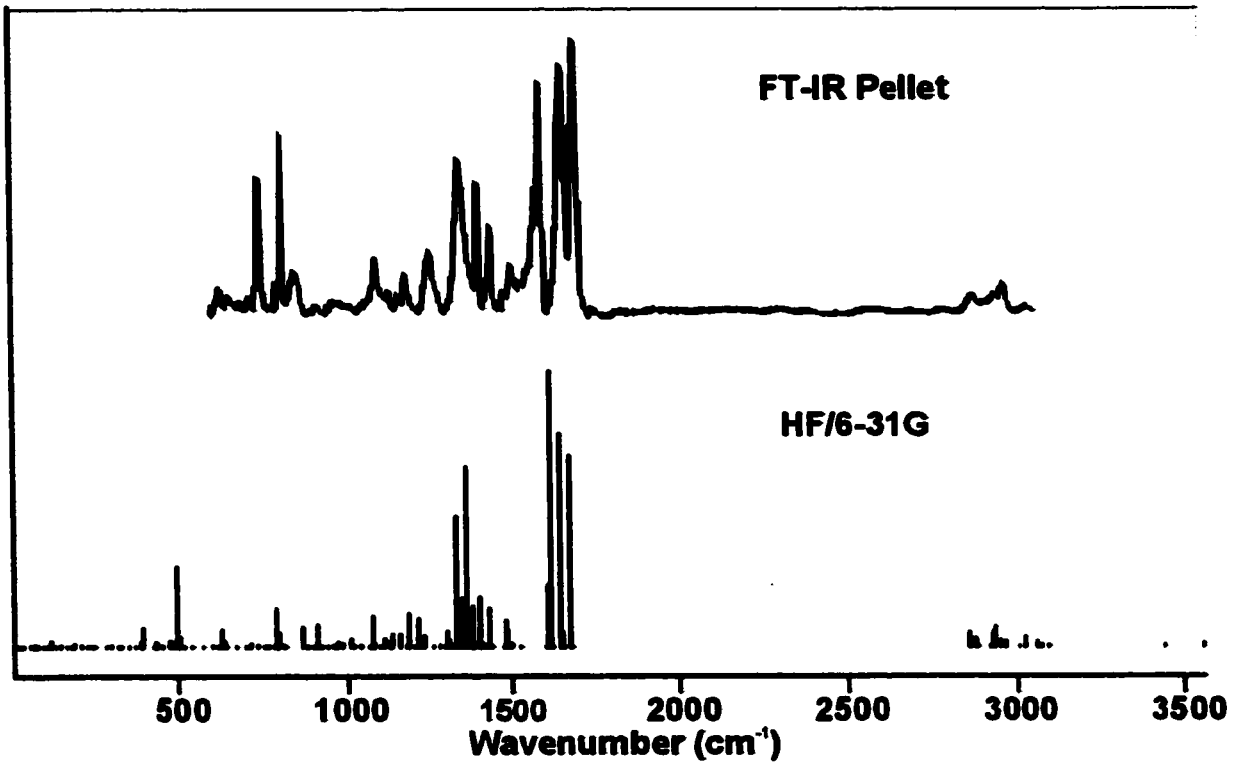

Figure 19: FT-IR of solid PTCD-NH_2 pellet and a calculated Hartree-Fock IR intensities.

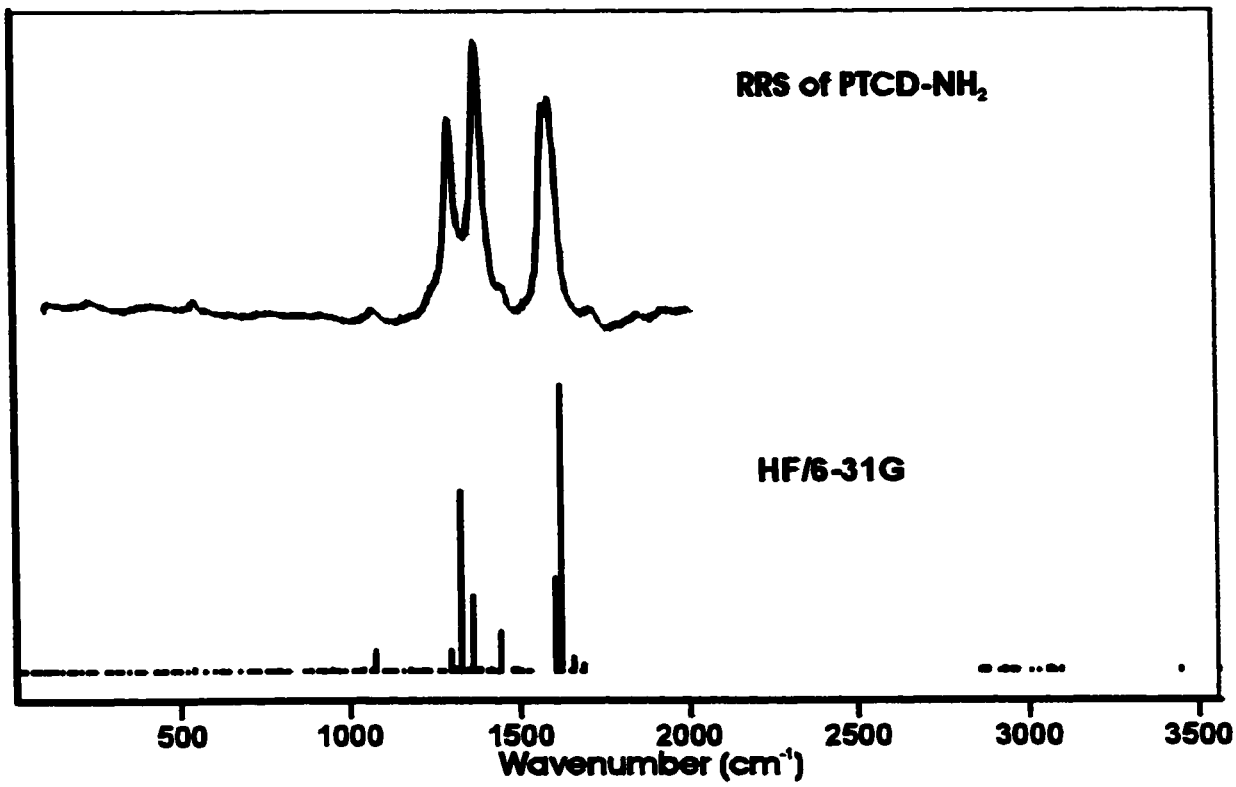

Figure 20: RRS spectra of solid PTCD-NH_2 powder with calculated Hartree-Fock Raman intensities.

Transmission FTIR spectra of PTCD-NH_2 dispersed in a KBr pellet and of thin solid films deposited on IR transparent substrates are shown in Figure 22, and observed wavenumbers are listed in Table 2. The characteristic vibrations of the perylene chromphore can easily be recognized in the spectra, and have been described in the literature.[64-67] The characteristic fundamentals will be discussed in more detail in the section where transmission and reflection-absorption (RAIRS) results are compared.

3.3.2. RAIRS

Transmission and reflection spectroscopic techniques can be used to determine the molecular orientation in thin organic films[68,69]. Greenler has shown that light at a reflecting surface is highly polarized, and at certain angle of incidence, the p-polarized component of the electromagnetic wave is three

orders of magnitude greater than the s-polarized or perpendicular component. The optical geometry of the reflection experiment is given in Figure 21. If a molecule is oriented such that the change in the dynamic dipole moment of one of its normal vibrational modes is parallel to the electric field ($\mu \bullet E$, with $\cos \angle (\mu \bullet E) = 1$) it shows a maximum in intensity. However, if the change in the dynamic dipole moment of the same vibrational mode is oriented perpendicular to the electric field, the resulting intensity would be negligible. Therefore, from the spectral data, the average molecular orientation can be extracted.

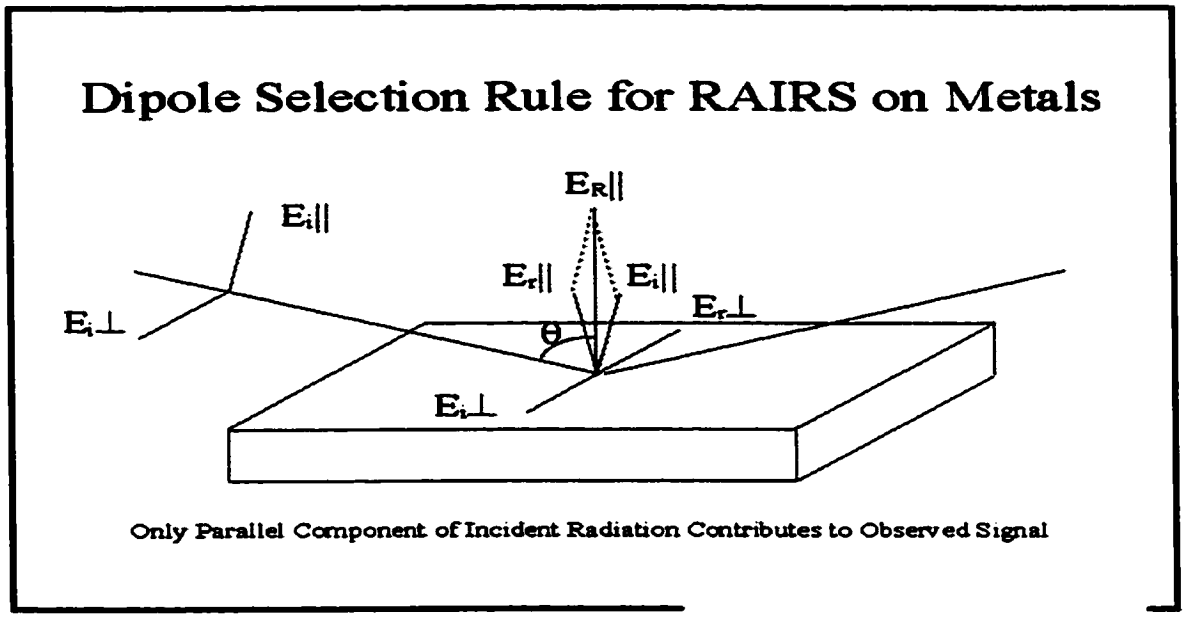

Figure 21. Electric field components in a RAIRS experiment on a mirror.

The transmission and RAIRS spectra of PTCD-NH_2 are shown in Figure 22. Typical C=C stretching vibrations of the perylene ring are observed at 1575 and 1593 cm^{-1}. The strong infrared bands centered at 1653 and 1694 cm^{-1} are assigned to the antisymmetric and symmetric C=O stretching vibrations, respectively. The band with stronger relative infrared intensity is the symmetric stretching at 1694 cm^{-1}. The prominent C-H out of plane modes are seen at 746 cm^{-1} and 810 cm^{-1}. Alkyl C-H stretching frequencies are observed at 2867, 2932 and 2959 cm^{-1}. Observed wavenumbers are collected in Table 1.

A careful examination of the three spectra of PTCD-NH_2 given in Figure 22 reveals important changes in the relative intensities of the internal ratio between the relative intensities of the in-plane of PTCD modes to that of the out-of the PTCD plane modes. Comparisons are made despite the fact we are using three different substrates, and the assumption here is that the substrate does not affect the molecular packing, i.e. the intermolecular interactions are stronger than the molecule substrate interactions. The pellet spectrum is used as a reference to determine molecular organization or preferential orientation in the evaporated films. Since the KBr pellet contains a random distribution of molecules in the sample, changes in relative intensity within the spectra of evaporated films may be attributed to partial organization of the molecules on the dielectric or reflecting substrates. According to the spectral data shown in Figure 22, the relative intensities of the two out of plane C-H wagging vibrations decreases with respect to the symmetric and antisymmetric C=O stretching vibrations in the RAIRS spectra. Therefore, a complete face-on orientation on the substrate can be rejected. The other possible orientations are head-on and edge-on. The area per molecule (15$Å^2$) occupied by PTCDNH_2 on a pure water suphase suggest a molecular packing with a head-on molecular orientation. The presence of comparatively modest intensity of C-H out-of–plane vibration in the KBr film together with a weak intensity in RAIRS, eliminate the complete edge-on orientation or head-on orientation. The fact that both carbonyl bands, symmetric and anti-symmetric, are observed with strong relative intensity excludes the

head-on orientation. The only reasonable conclusion is to assume that the PTCD-NH_2 molecule is tilted on the surface of the substrate preferentially. Based on the packing information extracted from the LB work, a tilted head-on orientation is most likely.

The infrared absorbance spectrum of a single LB monolayer deposited on germanium substrate obtained for PTCD-NH_2 molecule was also obtained and given in Figure 23. However, only the highest main perylene chromophore vibrations were observed in the spectrum. The characteristic of C=C stretching vibration and the two symmetric and antisymmetric C=O were well resolved and observed at 1595, 1700 and 1655 cm^{-1} respectively.

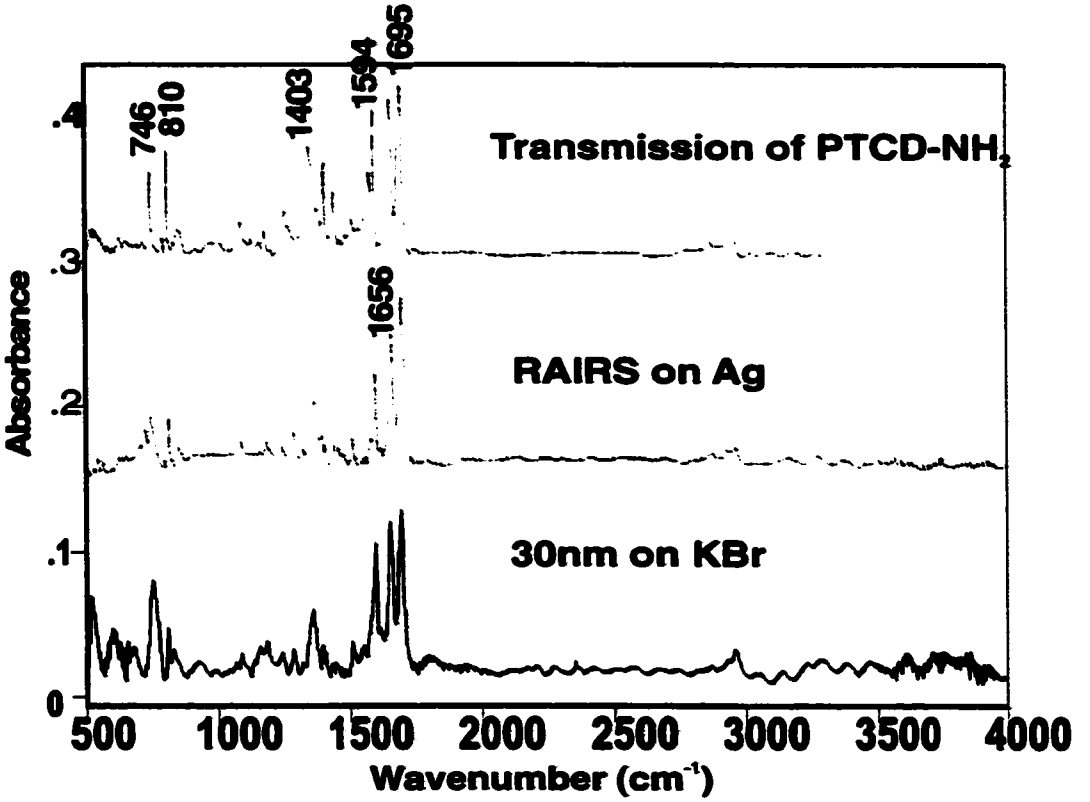

Figure 22: Transmission spectra of PTCD-NH_2 pellet and 100 nm KBr and RAIRS spectrum of an evaporated 100 nm film of PTCD-NH_2 on silver mirror.

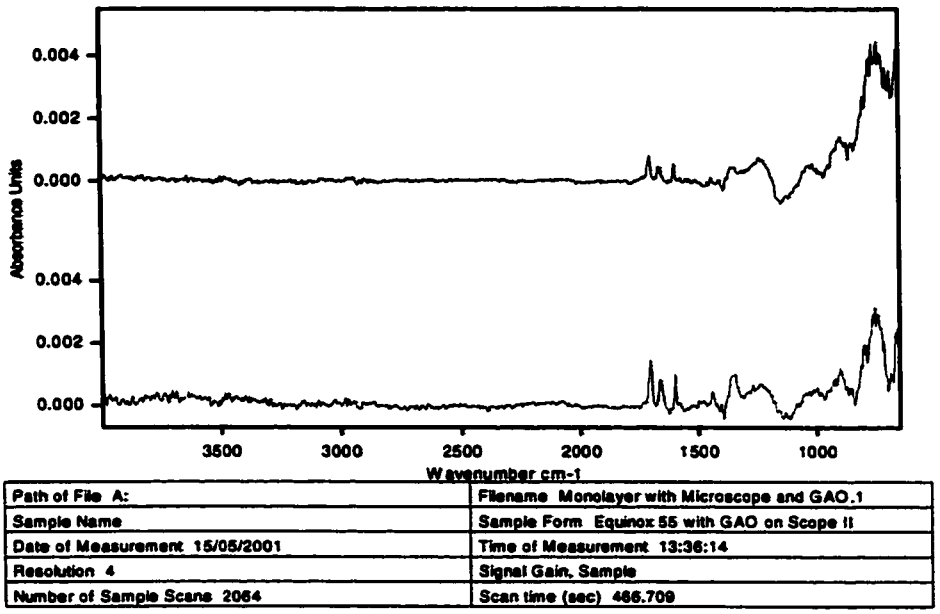

Figure 23: Infrared spectra of PTCD-NH_2 LB monolayer film

Table 1: Calculated and observed IR frequencies and relative intensities for PTCD-NH_2.S.F *= 0.9.

Calculated*	Intensity Km/mole	Pellet (cm^{-1})	RAIRS (cm^{-1})	Monolayer (cm^{-1})	Assignment
17	0				Ring def
19	0				Ring def
29	0				Ring def
33	0				Ring def
42	2				Ring def
59	6				Ring def
65	0				Butyl CH_3 torsion
72	4				NH_2 twisting
78	4				Ring def, NH_2 twisting
86	1				Ring def
100	1				Ring def

108	3				Alkyl CH_2 twisting
119	24				NH_2 scis
127	6				Ring def
133	1				NH_2 twisting
151	4				Ring C-H bending
171	0				Ring def, ring C-H wag
181	3				Ring def, ring C-H wag
190	11				Ring def, ring C-H wag
209	9				Ring def
226	0				Ring def, butyl CH_3 twisting
254	0				Ring def, butyl CH_3 twisting
248	3				Ring def, butyl CH_3 twisting
280	0				Ring def
297	8				Ring def
317	3				Ring def
324	2				Ring dist
325	0				Ring dist, ring C-H wag
350	2				Ring def
370	0				Ring def, alkyl CH_2 twisting
385	17				Ring def, alkyl CH_2 twisting
388	16				Ring def
389	0				Ring def
392	70				Ring def
424	0				Ring def
428	17				Ring def, alkyl rocking
436	13				Ring def
450	1				Ring def
456	0				Ring C-H wag
475	26				Ring C-H wag, NH_2 bending
479	16				Ring C-H wag, NH_2 bending
496	315				NH_2 wag

Calculated*	Intensity Km/mole	Pellet (cm^{-1})	RAIRS (cm^{-1})	Monolayer (cm^{-1})	Assignment
502	37				Ring def
520	0				Ring def
539	0				Ring breathing
540	0				Ring C-H wag
573	0				Ring def, ring C-H bending
603	7				Ring def
615	1				Ring def
627	67				Ring def
638	19				
639	0				Ring C-H wag
673	0				Ring C-H wag
702	0				Ring Def, ethylene CH_2 twist
708	3				Ring C-H Wag
713	11	746m	746vw		Ring def.
717	1				Ring def.
733	5				Butyl CH_2 Twisting
754	1				Butyl CH_2 Twisting
759	1				Ring C-H wag
768	0				Ring C-H wag
783	5				Butyl, ethylene CH_2 Twisting
788	152	792w	793vw		Ring C-H wag
792	2				Ring C-H wag
798	52				Ring def, ring C-H bending
814	9				Ring C-H wag
819	1				Butyl, ethylene CH_2 Twisting
867	81	810m	810w		Ring C-H wag
881	0				Ring C-H wag
882	2				Ring C-H wag
885	3				Ring C-H Wag, butyl CH_3 bending
903	3				Ring C-H Wagging

Calculated*	Intensity Km/mole	Pellet (cm^{-1})	RAIRS (cm^{-1})	Monolayer (cm^{-1})	Assignment
909	0				Ring C-H wag
914	87				Ring C-H wag
922	0				Ring C-H wag
926	2				Ring def, Butyl twisting Ethylene CH_2 twisting
942	3				Butyl CH_2 twisting
947	0				Ring C-H wag
962	7				Alkyl CH_2 twisting
987	12				Ring C-H bending, butyl CH_2 rocking
1010	28				Ring C-H bending, butyl CH_2 rocking Ethylene N-H bending
1023	0				Ring C-H bending
1035	2				Butyl CH_2 rocking
1038	4				
1064	0				Ring C-H wag
1067	0				Ring C-H wag
1068	0				Ring C-H wag
1069	0				Ring C-H wag
1075	120	1089m	1089vw		Ring C-H bend, Butyl rocking
1079	11				Ring C-H bend, butyl CH_2 bending
1099	3				Ring def, Alkyl CH_2 twisting

Calculated*	Intensity Km/mole	Pellet (cm^{-1})	RAIRS (cm^{-1})	Monolayer (cm^{-1})	Assignment
1106	30				Ring def, Alkyl CH_2 twisting
1121	19	1127vw	1127vw		Ethylene CH_2 twisting
1134	47	1146	1146		Ring C-H bending
1159	48	1157	1157		Ring C-H bending
1176	4				Ring C-H bending
1182	127	1181m	1181vw		Ring C-H bending
1187	1				Ring C-H bending
1203	1				Ring C-H bending
1210	111	1253w	1254vw		Ring C-H bending
1220	5				Ring C-H bending
1231	43				Ring C-H bending
1233	30				Ring C-H bending
1281	8				Ring C-H bend, alkyl CH_2 bending
1297	3				Ring C-H bending
1299	61				Alkyl CH_2 twisting, N-H bending
1308	5				Ring C-H bending
1310	13				Ring C-H bend, ethylene CH_2 rocking
1311	22				Alkyl CH_2 twisting

Calculated*	Intensity Km/mole	Pellet (cm^{-1})	RAIRS (cm^{-1})	Monolayer (cm^{-1})	Assignment
1319	0				Ethylene CH_2 twisting
1325	8				Ring C-H bending
1331	503				Ring deformation Ring C-H bending
1337	7				Butyl CH_2 twisting
1349	188				Ring C-H bending, butyl CH_2 bending
1360	8				Ring C-H bending, ring deformation
1365	694	1348s	1348w		Ring deformation
1375	77				Ethylene CH_2 twisting
1382	155				Alkyl Twist
1383	103				Alkyl CH_2 Twist
1386	15				Alkyl CH_2 rocking, ring C-H bending
1408	7				Alkyl CH_2 rocking
1413	10				Alkyl CH_2 rocking
1422	4				Ethylene CH_3 scissoring
1435	148	1440s	1440vw		Ring str.
1443	1				Ring str.
1477	0				Ring C-H bending
1481	104				Alkyl C-H bending
1485	66				Ethylene CH_2 scissoring

Calculated*	Intensity Km/mole	Pellet (cm^{-1})	RAIRS (cm^{-1})	Monolayer (cm^{-1})	Assignment
1487	1				Ethylene CH_2 bending, CH_3 scissoring.
1491	6				Ethylene CH3 bending.
1492	8				Ethylene CH_3 twisting
1493	11				Ring C-H bending
1501	4				Butyl CH_2 scissoring
1502	14	1504vw	1507vw		Ethylene CH_2 scissoring
1524	0				C-H bending
1526	0				Ring C-H bend, C=C str.
1603	0				C = C str
1608	190	1575w	1575vw		Ring dist, C-H bending, C=C str.
1610	241				
1618	250				Ring def, C-H bending
1624	0				Ring def, C-H bending
1648	831	1651vs	1653vs		C=O Antisymmetric out of phase str.
1656	57	1655vs	1655vs	1655vs	C=O Antisymmetric out of phase str.
1660	1				N-H scis, ring def.
1680	737	1694vs	1696s	1700vs	C=O antisymmetric out of phase str, alkyl C-H bending, N-H bending

1684	1				C=O symm str. Alkyl CH_2 bend, N-H bending
2856	37				Ethylene CH_2 symm str
2858	52	2867w	2867vw		Butyl CH_2 symm str.
2865	33				Ethylene CH_3 , CH_2 symm str
2877	30				Ethylene CH_2 symm str.
2881	8				Alkyl C-H Antisymm Str
2915	2				Ethylene CH_2 symm str
2929	63				Ethylene CH_3 antisymm str.
2930	81	2932vw	2932vw		Ethylene CH_3, CH_2 antisymm str
2932	18				Butyl CH_2 antisymm str.
2953	22	2959w	2959w		Butyl CH_2 antisymm str.
2968	17				Ethylene CH_2 symm str
3007	3				Butyl CH_2 symm str
3027	34				Ethylene CH_2 antisymm str.
3059	19				Butyl CH_2 antisymm str.
3060	0				Ring C-H in-phase symm str.
3066	0				Ring C-H in phase symm str.
3066	2				Ring C-H in phase symm str.
3075	0				Ring antisymm C-H str.

3075	5				Ring C-H out of phase str.
3095	9				Ring C-H symm str.
3095	5				Ring C-H symm str.
3444	8				NH_2 symm str.

Table 2 : Calculated and observed Raman frequencies and relative intensities for PTCD-NH_2. S.F *= 0.9[70]

Calculated*	Intensity	Powder RRS (cm^{-1})	LB Monolayer SERRS (cm^{-1})	Assignment
17	1			Ring def
19	1			Ring def
29	2			Ring def
33	3			Ring def
42	0			Ring def
59	0			Ring def
65	0			Butyl CH_3 torsion
72	1			NH_2 twisting
78	0			Ring def, NH_2 twisting
86	0			Ring def
100	0			Ring def
108	0			Alkyl CH_2 twisting
119	2			NH_2 scis
127	0			Ring def
133	1			NH_2 twisting
151	1			Ring C-H bending
171	0			Ring def, ring C-H wag
181	0			Ring def, ring C-H wag
190	0			Ring def, ring C-H wag
				Ring def
209	0			Ring def, butyl CH_3 twisting
226	3			Ring def, butyl CH_3 twisting
254	11			Ring def, butyl CH_3 twisting
280	0			Ring def
297	0			Ring def
317	3			Ring dist

324	2			Ring dist
325	0			Ring dist, ring C-H wag
350	2			Ring def, alkyl CH_2 twisting
370	24			Ring def, alkyl CH_2 twisting
385	1			Ring def, alkyl CH_2 twisting
388	4			Ring def
389	10			Ring def
392	0			Ring def
424	15			Ring def
428	16			Ring def, alkyl rocking
436	0			Ring def
450	15			Ring def
456	16			Ring C-H wag
475	5			Ring C-H wag, NH_2 bending
479	12			Ring C-H wag, NH_2 bending
489	1			Ring C-H bending
496	7			NH_2 wag
502	9			Ring def
520	3			Ring def
539	121		545 (5)	Ring def
540	9			Ring C-H wag
573	23			Ring def, ring C-H bending
603	0			Ring def
615	4			Ring def
627	2			Ring def
638	0			
639	0			Ring C-H wag
673	0			Ring C-H wag

Calculated*	Intensity	Powder RRS (cm^{-1})	LB Monolayer SERRS (cm^{-1})	Assignment
708	1			Ring C-H Wag
713	1			Ring def.
717	28			Ring def.
733	0			Butyl CH_2 twisting
754	0			Butyl CH_2 twisting
759	1			Ring C-H wag
768	0			Ring C-H wag
783	3			Butyl, ethylene CH_2 twisting
788	1			Ring C-H wag
792	3			Ring C-H wag
798	0			Ring def, ring C-H bending
814	1			Ring C-H wag
819	3			Butyl, ethylene CH_2 twisting
867	0			Ring C-H wag
881	33			Ring C-H wag
882	13			Ring C-H wag
885	25			Ring C-H wag, butyl CH_3 bending
903	9			Ring C-H wag, butyl CH_3 bending
909	1			Ring C-H wag
914	0			Ring C-H wag
922	0			Ring C-H wag
926	0			Ring def, Butyl twisting Ethylene CH_2 twisting

Calculated*	Intensity	Powder RRS (cm^{-1})	LB Monolayer SERRS (cm^{-1})	Assignment
947	48			Ring C-H wag
962	5			Alkyl CH_2 twisting
973	3			Ring C-H bending, Butyl CH_2 rocking
987	20			Ring C-H bending, butyl CH_2 rocking
1010	10			Ring C-H bending, butyl CH_2 rocking Ethylene N-H bending
1023	22			Ring C-H bending
1035	25			Butyl CH_2 rocking
1038	45			
1064	0			Ring C-H wag
1067	0			Ring C-H wag
1068	121			Ring C-H wag
1075	120			Ring C-H bend, butyl rocking
1079	842			Ring C-H bend, butyl CH_2 bending
1099	6			Ring def, Alkyl CH_2 twisting
1106	1			Ring def, Alkyl CH_2 twisting
1121	14			Ethylene CH_2 twisting
1134	0			Ring C-H bending
1159	0			Ring C-H bending

Calculated*	Intensity	Powder RRS (cm^{-1})	LB Monolayer SERRS (cm^{-1})	Assignment
1176	82			Ring C-H bending, alkyl CH_2 twisting, ring distortion.
1182	7			Ring C-H bending, alkyl CH_2 twisting
1187	41			Ring C-H bending
1203	4			Ring C-H bending
1210	0			Ring C-H bending
1220	21			Ring C-H bending
1231	0			Ring C-H bending
1233	20			Ring C-H bending, ethylene CH_2 twisting
1263	11			Ring C-H bend, alkyl CH_2 bending
1297	856			Ring str. C-H bending
1299	36			Ring st , C-H bending
1308	1			Ring C-H bending
1310	114			Ring C-H bend, ethylene CH_2 rocking
1311	21			Alkyl CH_2 twisting
1319	25			Ethylene CH_2 twisting

Calculated*	Intensity	Powder RRS (cm^{-1})	LB Monolayer SERRS (cm^{-1})	Assignment
1325	7752	1298 (100)	1298 (100)	Ring sstr.
1331	54			Ring deformation Ring C-H bending
1337	12			Butyl CH_2 twisting
1349	53			Ring C-H bending, butyl CH2 bending
1360	3198	1376(83)	1376(94)	Ring C-H bending, ring str.
1365	10			Ring deformation
1375	61			Ethylene CH_2 twisting
1382	16			Alkyl twisting
1383	41			Alkyl CH_2 twisting
1386	56			Alkyl CH_2 Rocking, ring C-H bending
1401	3			Ring in- plane str, C-H bending
1408	35			Alkyl CH_2 Rocking
1413	54			Alkyl CH_2 rocking
1422	18			Ethylene CH_3 scissoring
1435	7			Ring C-H bend, alkyl C-H bending
1443	1729	1454 (7)	1454 (11)	Ring str.
1477	81			Ring C-H bending

Calculated*	Intensity	Powder RRS (cm^{-1})	LB Monolayer SERRS (cm^{-1})	Assignment
1481	28			Alkyl C-H bending
1485	5			Ethylene CH2 scissoring
1488	47			Ethylene CH_2 bending, CH_3 scissoring.
1491	20			Ethylene CH_3 bending.
1492	26			Ethylene CH_3 twisting
1493	0			Ring C-H bending
1501	10			Butyl CH_2 scissoring
1502	1			Ethylene CH_2 scissoring
1524	1			C-H bending
1526	0			Ring C-H bend, C=C str.
1603	3996	1571 (36)	1571 (36)	Ring str.
1608	0			Ring dist, C-H bending, C=C str.
1610	0			Ring def, C-H bending
1618	76			Ring def, C-H bending
1624	12373	1586 (95)	1586 (74)	Ring str.
1648	0			C=O Antisymmetric out of phase str.
1656	14			N-H bending
1660	623			N-H bend, ring def.

Calculated*	Intensity	Powder RRS (cm^{-1})	LB Monolayer SERRS (cm^{-1})	Assignment
1684	251			C=O symm str. Alkyl CH_2 bend, N-H bending
2856	53			Ethylene CH_2 symm str
2858	62			Butyl CH_2 symm str.
2865	146			Ethylene CH_3 , CH_2 symm str
2877	62			Ethylene CH_2 symm str.
2881	116			Alkyl C-H Antisymm Str
2915	1			Ethylene CH_2 symm str
2929	154			Ethylene CH_3 antisymm str.
2930	36			Ethylene CH_3, CH_2 antisymm str
2953	69			Butyl CH_2 antisymm str
2968	74			Ethylene CH_2 symm str
3007	29			Butyl CH_2 symm str
3027	34			Ethylene CH_2 antisymm str.
3059	0			Butyl CH_2 antisymm str.
3060	124			Ring C-H in-phase symm str.
3066	125			Ring C-H in-phase symm str.
3066	2			Ring C-H in phase symm str.

3075	33			Ring C-H in phase symm str.
3075	3			Ring antisymm C-H str.
3095	103			Ring C-H symm str.
3444	148			NH_2 symm str
3556	89			NH_2 antisymm. str.

3.4. Resonance Raman Scattering

The vibrational spectra of PTCD molecules have been discussed for a series of related materials. [68]. The RRS contains a small number of characteristic molecular wavenumbers listed in Table 3, which are observed for a series of perylene derivatives[71-73] . The resonance Raman spectra of the neat powder were obtained using a 514.5 nm excitation line, and were dominated by the typical perylene chromophore spectra. The Raman peak positions are basically the same as those of the SERRS spectra, except that there are small differences in FWHM (full width at half-maximum), as shown in Table 3. In Figure 24, the relative intensities of the perylene ring stretches at 1376, 1454 and 1586 cm^{-1} changed relative to the SERRS spectra of the monolayer film.

3.4.1. Surface Enhanced Raman Scattering

The SERS and SERRS of perylene and its derivatives have been reported in a number of many publications. [74,75] Surface enhanced Raman scattering (SERS) of PTCD-NH_2 were obtained using 780 and 633 nm laser lines which are off resonance of the PTCD-NH_2 electronic absorption. Figure 24 shows the Raman spectra of the neat powder, LB film and analyte suspended in colloid silver solution.

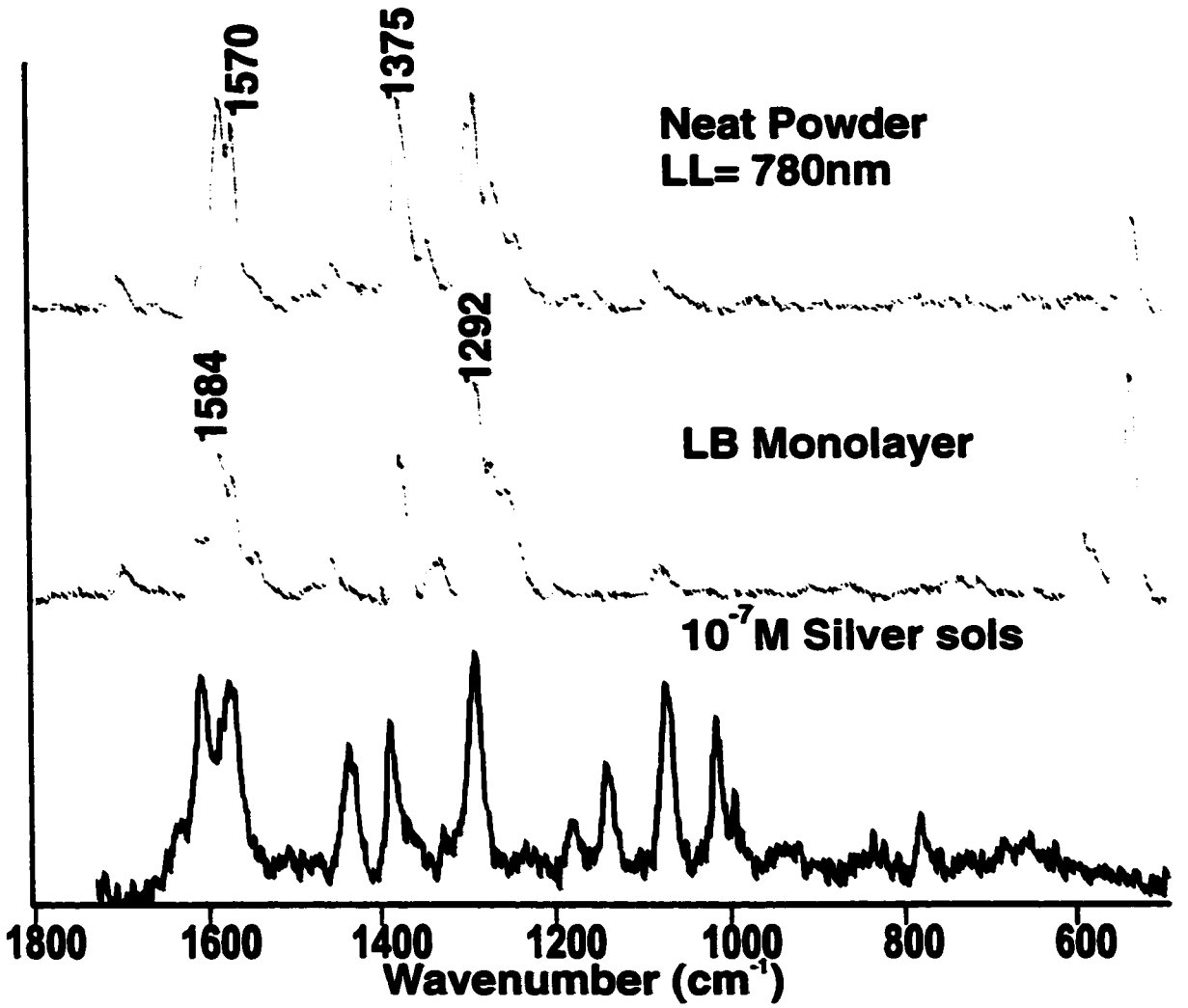

Figure 24: The SERS spectra of PTCD-NH_2 neat powder, LB film and colloid solution.

The normal Raman spectrum of solid PTCD-NH_2 in the frequency range of 400-1800 cm^{-1} is shown in Figure 24. The Raman peak positions on all the substrates are basically the same, except there are small shifts for the LB monolayer film using LL=780 nm. As shown in Figure 25, the relative intensity of the SERS peaks of the PTCD-NH_2 molecules changed considerably when different excitation wavelengths, λ, were used. Similar effects of λ were observed for the solution spectra. For λ= 633 nm or closer to resonance, the peak at 1299 cm^{-1} gains a maximum intensity.

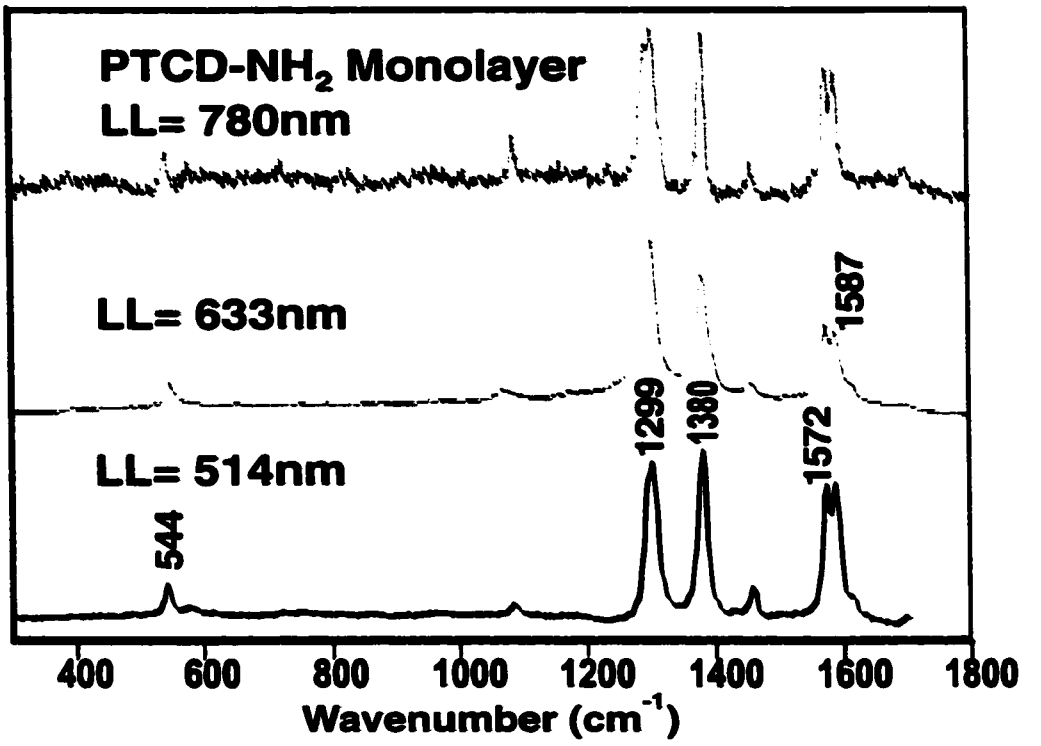

Figure 25: SERS and SERRS spectra of LB monolayer film.

For λ= 780 nm the two peaks at 1299 and 1380 cm^{-1} the intensities are almost equal. And also the signal to noise ratio was higher for the laser line λ=780 nm compared with λ=633 nm. Hence, this shows that the absolute intensity increase as resonance approached.

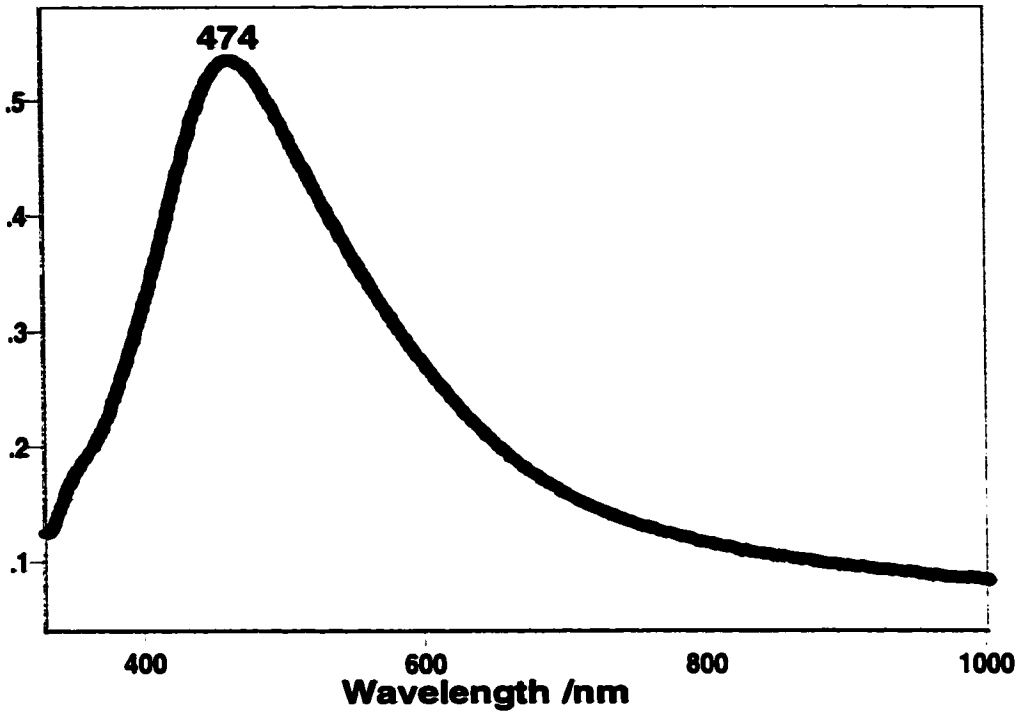

Figure 26: The plasmon absorption of 6 nm silver film on glass

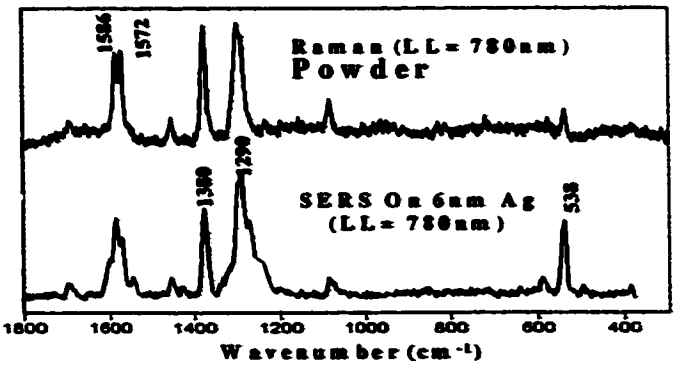

Figure 27: Normal Raman and SERS spectra of PTCD-NH_2

3.4.2. Surface Enhanced Resonance Raman Scattering Spectroscopy: Fundamentals and overtones.

SERRS quenches fluorescence and enhances Raman scattering for adsorbed molecules on a roughened metal surface or silver colloid .The SERRS spectra of PTCD-NH_2 contains a small number of characteristics fundamentals that can be attributed to the chromophore moiety. The spectra shown in Figure 28 were collected from the three substrates using 514.5 nm excitation line. The spectra were collected in 10s integration time with less than 1mW of laser power at the LB monolayer and the evaporated films sample. A maximum power of 1mW was used for the colloid solutions.

PTCD-NH_2 can easily be attached on silver sols and silver islands. This phenomenon of (chemical adsorption) observed through the change of the colloid color from yellow to colorless. In spite of this, no apparent shifts in wavenumber or differences were observed in the SERRS spectra. Figure 29 shows the SERRS spectra of the LB monolayer film and 10 nm evaporated film. The bands at 1587 and 1572 cm^{-1} are the prominent feature of the C=C stretching modes. The other prominent bands at 1299 and 1378 cm^{-1} are assigned for C-H bending and ring stretching correspondingly. A ring distortion mode is observed at 545 cm^{-1}. Table 3 gives the vibrational assignments for the measure peaks and the theoretical calculation.

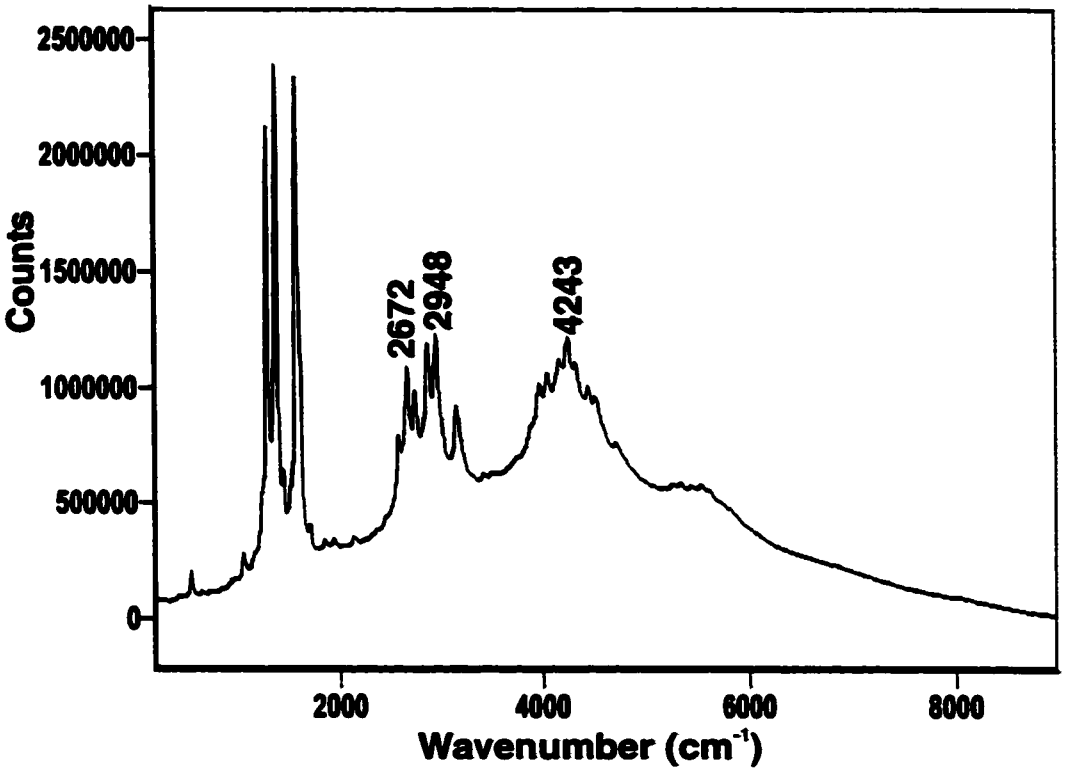

Figure 28: SERRS of LB monolayer film of PTCD-NH_2 recorded with 514.5 nm laser line. The overtones and combination are shown.

Table 3: Overtones and combinations bands observed in the SERRS spectrum of PTCD-NH_2 excited with 514.5 nm laser line.

Observed (cm^{-1})	Overtones and Combinations
2131	1063 X 2 = 2126
2589	1291 X 2 = 2582
2672	1291 + 1377 = 2668
2752	1377 X 2 = 2754
2870	1291 + 1572 = 2863
2948	1377 + 1572 = 2949
3150	1572 X 2 = 3144
3424	1572 + 1850 = 3422
3505	1572 + 1934 = 3506
3890	1291 + 2589 = 3880
3970	1377 + 2589 = 3966
4046	1934 + 2134 = 4068
4162	1572 + 2589 = 4161
4243	1291 + 1377 + 1572 = 4240
4317	(1377 X 2) + 1572 = 4326
4444	1572 + 2870 = 4442
4518	1572 + 2948 = 4520
4718	2131 + 2589 = 4720
5255	2672 + 2589 = 5261
5333	2672 X 2 = 5344
5429	
5527	
5603	
5710	
5808	

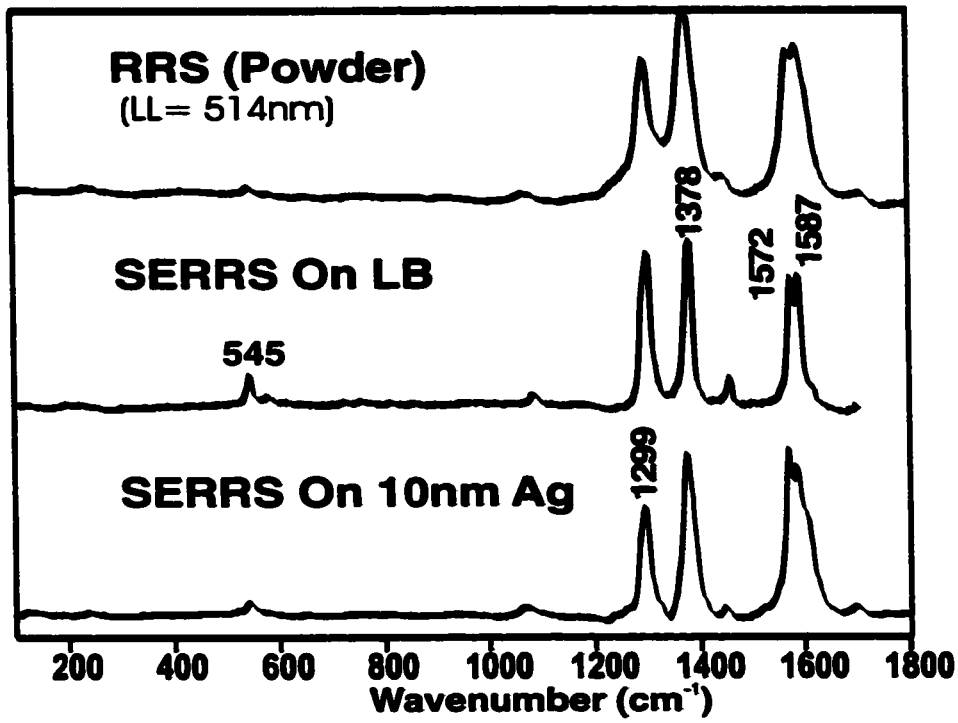

Figure 29: RRS and SERRS spectra of an LB film of PTCD- NH_2

The reduction of silver using citrate produces a colloid with particles sizes in ranges of (3 to 87 nm) Figure 8. The wavelength of maximum absorbance is (λ_{max}=404 nm). The SERRS spectra of PTCD-NH_2 in the silver solution are displayed in Figure 30 in the absence of halide ions. The SERRS/RRS enhancement factor roughly estimated is ~ 10^3, which is in a good agreement with the prediction based on the theoretical treatment of the SERRS effect.[76]

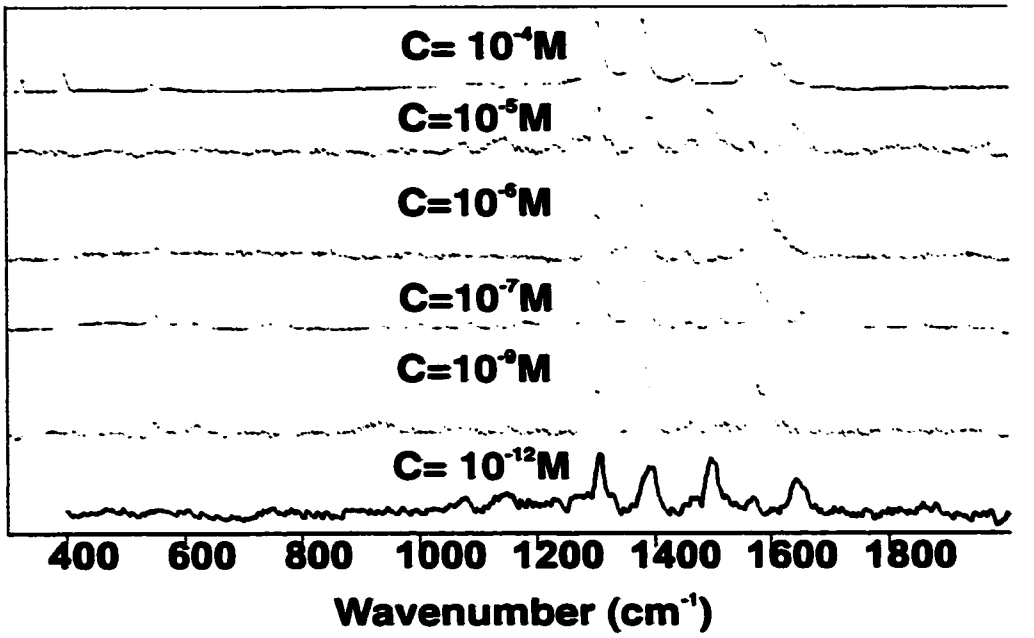

Figure 30: SERRS spectra of colloidal sol immobilized on polysilane substrate.

4.0. SINGLE MOLECULE DETECTION OF PTCD-NH_2

4.1. Single Molecule Detection on Colloidal Silver

Single molecule detection (SMD) is achieved through the multiplicative effect of two enhancement factors provided by the resonance Raman effect and the surface-enhanced Raman effect that increases the effective Raman cross section to a detectable level [77]. Under the appropriate conditions the detection of a single molecule within the probed volume or surface area can be achieved.

Silver colloids were used in the first set of experiments leading to SMD results. Silver colloids were prepared by the citrate-reduction method according to the description of Lee and Meisel[46] and diluted with water in a 1:7 ratio. The sols prepared under these conditions were stable, and there was no indication of precipitation or color changes for several months. The citrate colloid used, presents a typical plasmon absorption in the visible (center at ca. 405 nm), as

was shown in Figure 7. The neat colloid, when allowed to dry on a glass surface, forms, by aggregation typical fractal structures (as can be seen in the inset of Figure 8) that have been shown to have peculiar enhancing properties [78]. An AFM study shows that in the original colloids there is a wide distribution of particle sizes centered at low particle size (ca. 20 nm).The topographical, and lateral force AFM pictures of the silver nanoparticles of dilute silver sols are shown in Figure 9-11.

For SERRS measurements, an aliquot of $PTCDNH_2$ solution was transferred with a clean micro syringe to silver colloid, to achieve an overall concentration of the analyte ranging from 10^{-6} M down to 10^{-12} M. The substrates used to hold the water droplets were polysilane-coated glass, quartz, and germanium slides. The silver colloids were not "activated" with chloride ions as is commonly done in colloidal SERS work[79]. A second set of samples were allowed to dry for micro-Raman measurements. For the liquid sample, an oil immersion (40X N= 0.80) objective was brought into direct contact with the droplet for excitation and collection of the scattered light. However, for the dried sample a 50x (N=0.75) objective was used for acquisition of the Raman spectra. Using concentrations in the 10^{-9} to 10^{-12} M regime of PTCD-NH_2, 65 µL of colloid solution was mixed with 30 µL of the PTCD-NH_2 solution. Therefore the total number of molecules in 30 µL is 10^{-12} x 30 10^{-6} or 3 x 10^{-17} M, i.e., 30 attomole of analyte in the total volume of 95 µL. The silanization of the slides was done by immersion of the clean slides in freshly prepared 10^{-3} M octadecyltrichlorosilane (OTS) solution in toluene for 10 minutes. The OTS reacts with the adsorbed water on the surface of the film to produce an ill-defined cross linked polysiloxane coating[80]. The PTCD-NH_2 molecule has a $-CH_2$-CH_2-NH_2 terminal group attached to the PTCD aromatic core, and when added to the silver sols produces an aggregation of the colloidal particles that is seen by a change in the coloration of the colloidal solution. This is indirect evidence of chemical adsorption of PTCD-NH_2 onto the silver surface. The SERRS spectra, collected using the immersion lens, in colloidal solution samples containing a total of 30 attomoles of the dye, are shown in Figure 31. Assuming a scattering volume of 1 picoliter, the SERRS in

the 10^{-12} M solution comes from about 1 molecule within the illuminated area. Samples prepared by casting the 10^{-9} to 10^{-12} M solutions, onto the silanized surface, yield an average surface coverage of ca. 100 to less than 1 molecule per μm^2 of surface. The SERRS spectra of a casted sample are also presented in Figure 32. Notably, the band at 1300 cm^{-1} is observed in the spectra recorded with the immersion lens in the droplet and that of the bulk colloids. However, the in SERRS spectrum of the dried silver colloid the band is at 1294 cm^{-1}. It can also be seen that the SERRS spectra of the samples in the single molecule regime have a distinct pattern of relative intensities; where the 1294 cm^{-1} Raman band carries a lower relative intensity than in the bulk or "average" SERRS spectra.

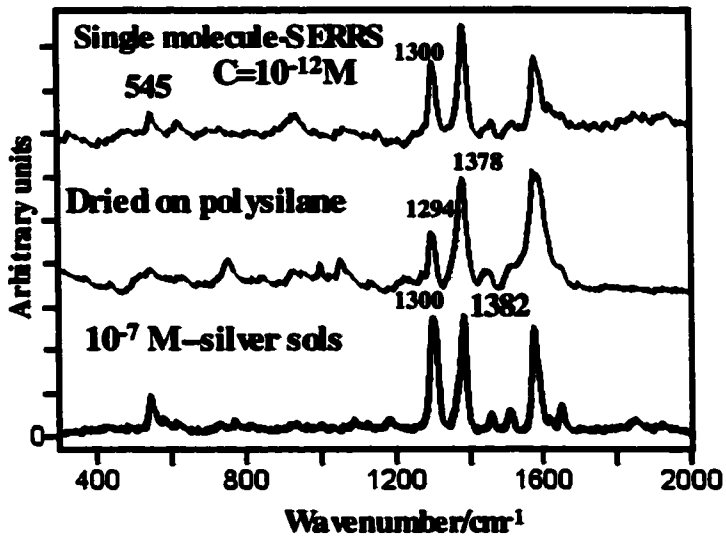

Figure 31: SERRS spectra of single molecule in silver solution and dried on polysilane substrate.

4.2. SMD on LB Monolayer

The concentrations of the spreading solution for Langmuir film preparation were calculated to achieve, on average, 1 to 100 molecules of PTCD-NH_2[81]. The AA (312.55 g mol^{-1}) solution was prepared directly by weighing 14.90 mg and diluting it in a 100mL volumetric flask. The PTCD-NH_2 (489.53 g mol^{-1}) solution was prepared by 2 dilutions from a more concentrated solution whose initial concentration was 9.80 X 10^{-4} mol L^{-1} (18.24 mg in 100 mL). The second dilution was done in the same flask as AA. The PTCD-NH_2 solutions were prepared using 10% trifluoroacetic acid (TFA) and 90% dichloromethane spectroscopic grade solvents. TFA is necessary since PTCD-NH_2 is not soluble in conventional organic solvents. All the flasks and micro

syringes used were cleaned with neutral detergent, chromic acid and acetone. After each step doubled distilled and deionized water were used. The spread solution was then left for approximately thirty minutes so that the solvent evaporated. Once the solvent had evaporated, the film was compressed at 20 mm min^{-1} by a single barrier from an area of 150 mm (trough width) X 187 mm (distance between the barrier and the sensor pressure) = 2.81 X 10^4 mm^2. The LB monolayer was deposited by immersing the substrate into the water subphase, then spreading the solution and waiting for the solid phase to stabilize, and finally lifting the substrate at 3.8 mm min^{-1} (Z-deposition). The transfer ratio, defined as the area due to the displacement of the substrate covered during the deposition was ca. 1.

In these experiments, direct transfer of colloidal silver nanoparticles onto the monolayer film was attempted by immersing the glass slide with LB film containing the dye into the colloidal solution. The silver nanoparticles that may have adhered to the LB film do not give detectable SERRS of the dye in the AA-dye monolayer. Therefore, an overlayer of 6nm of silver was evaporated onto the LB film with colloidal silver nanoparticles to achieve the SERRS spectrum. The reference SERRS spectrum of the neat LB monolayer of PTCD-NH_2 deposited on silver island films is shown in Figure 32. The fundamental vibrational wavenumbers of PTCD-NH_2 are clearly observed below 1700 cm^{-1}. First overtones and combinations are observed in SERRS with strong relative intensity. Second and third overtones are also observed and they are illustrated in Figure 32. The PTCD-NH_2 Raman spectrum is characteristic of what is normally seen in these materials, where, for a large molecular system, only a handful of fundamental vibrations of the chromophore are observed: 555 cm^{-1}, 1294 cm^{-1}, 1378 cm^{-1}, 1446 cm^{-1} and 1577 cm^{-1}. Overtones and combinations are progressions of these fundamental modes, as can be seen in Figure 32, where the intensity of the second and third overtones and combinations have been artificially enhanced for better viewing. The characteristic band at 1294 cm^{-1} is identified by the letter **a** in Figures 32 and 33. Similarly the Raman band at 1378 cm^{-1} is marked with the letter **b**.

PTCD-NH_2 secondary emission is characterized by strong excimer fluorescence that can also be enhanced on metal island films, producing surface enhanced fluorescence (SEF). Fluorescence is evident in the SERRS of neat films, and Raman scattering is observed with a strong fluorescence background. However, the fluorescence is completely quenched when the single molecule regime is approached. Therefore, no fluorescence background was observed in the SERRS on silver colloid, or in the SERRS of mixed LB with colloidal silver and a silver overlayer.

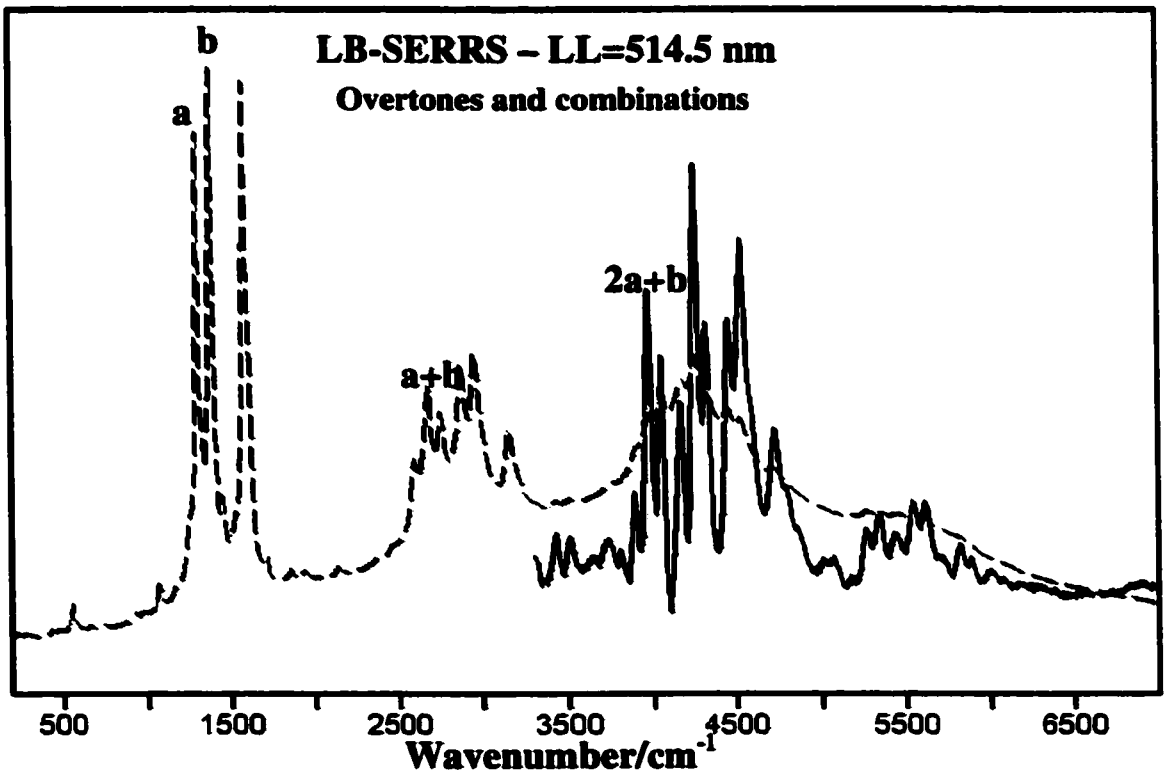

Figure 32: Reference SERRS spectrum of a single LB monolayer on silver island film. First, second and third overtones and combinations are also shown with an arbitrary intensity.

The spatially resolved SERRS spectra for LB monolayer containing 10 and 100 molecules per micron square, (the irradiated area in the Raman

microscope), are presented in Figure 33. Notably, the first overtones and combinations are also clearly observed in the single molecule SERRS spectra.

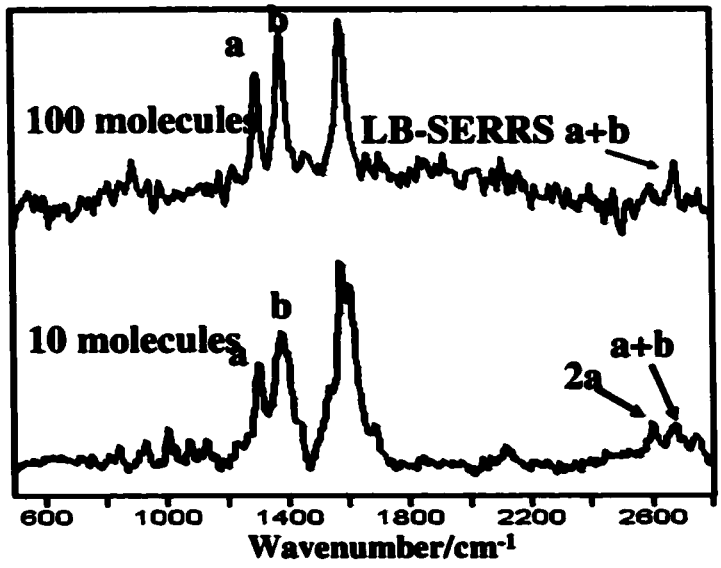

Figure 33: SERRS spectra of PTCD-NH_2 dispersed in an LB monolayer containing 10 and 100 molecules per μm^2.

The observation of overtones and combinations in the secondary emission gives very strong support for the vibrational assignment and origin of the observed Raman bands. The spectra show the same relative intensity pattern found in colloidal SERRS, and these support the assumption of single molecule SERRS made in the colloidal experiment. There are several important differences between the single molecule LB-SERRS and the neat PTCD-NH_2 LB monolayer on silver islands, or RRS spectra of LB on glass, in all three band parameters: relative intensities, full width at half maximum (FWHM) and wavenumber. These differences are illustrated in Table 4. The 1378 cm^{-1} band is seen with a higher relative intensity than the 1294 cm^{-1} band, in the single molecule LB monolayer spectrum. The opposite is observed in all the RRS and SERRS spectra for the neat PTCD-NH_2 LB monolayers. Notably, the calculated Raman intensities for PTCD-NH_2 (HF/6-31G) gives a larger absolute intensity for

the band assigned to the 1378 cm^{-1} in comparison with 1294 cm^{-1} band as can be seen in Figure 33. The FWHM of the single molecule LB monolayer spectrum is larger than the FWHM of the neat LB monolayer SERRS or RRS spectra. It was observed that for single molecule measurements, the observed wavenumbers show minor variations from spot to spot. It is well known that the SERRS spectra of neat PTCD contain a strong excimer emission signal due to SEF, and that excimer emission can only be observed in the presence of aggregates. Fluorescence spectra were recorded exciting a neat PTCD-NH_2 LB monolayer on silver islands with the 514.5 nm laser line and extending the scanning in the Stoke's region to 9000 cm^{-1}, where excimer emission (or SEF) was clearly observed. The SERRS bands in Figure 34 are observed on the background of excimer fluorescence of aggregates. Since excimer emission (and SEF) can be observed solely in the presence of aggregates, it may be concluded that the absence of any excimer emission in the single molecule SERS LB monolayer spectrum is experimental evidence for the lack of PTCD-NH_2 aggregates.

Table 4: Characteristic Raman bands observed in RRS spectrum of PTCD-NH_2 powder, LB-SERRS of a single monolayer on silver, and mixed LB with 1 and 100 dye molecules/μm^2.

Samples	Rel. Intensity	Center (cm^{-1})	FWHM (cm^{-1})	Interpretation
Powder RRS	1298	100	21	Ring str. + C-H bending
	1376	83	16	Perylene ring str.
	1454	7	8	Perylene ring str.
	1571	36	11	Perylene ring str.
	1586	95	23	Perylene ring str.
LB Monolayer SERRS	1298	100	23	Ring str. + C-H bending
	1376	94	21	Perylene ring str.
	1454	11	15	Perylene ring str.
	1571	36	15	Perylene ring str.
	1586	74	24	Perylene ring str.
LB 100 Molecule SERRS	1296	57	24	Ring str. + C-H bending
	1377	94	30	Perylene ring str.
	1454	7	19	Perylene ring str.
	1577	100	32	Perylene ring str.
1 Molecule SERRS	1299	66	24	Ring str. + C-H bending
	1380	100	39	Perylene ring str.
	1572	85	23	Perylene ring str.
	1604	66	30	Perylene ring str.

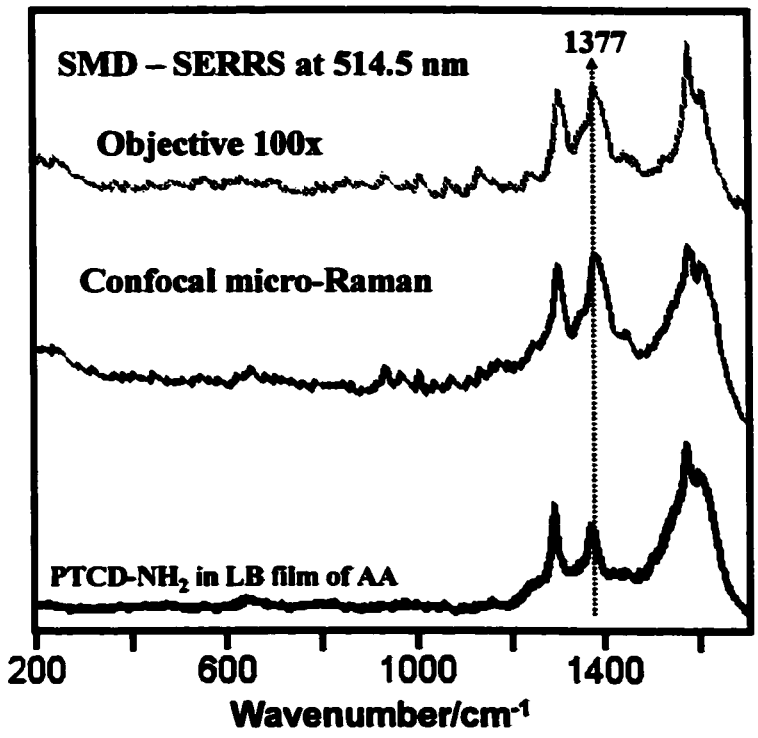

Figure 34: SERRS spectra of PTCD-NH_2 dispersed in an LB monolayer containing 1 molecule per μm^2. At the top is single molecule spectrum collected with a 100X objective (NA 0.9). In the middle is the confocal spectrum recorded with the 50X objective, and at the bottom is a spectrum collected with 50X objective.

The single molecule spectra were also recorded using the confocal microscopy set up available in the Renishaw 2000 (slit adjustment) in order to reduce the amount of light coming from the field of observation. The SERRS spectrum obtained is shown in Figure 33. For comparison the same spectral region collected with the 100x objective and without confocal adjustment is also shown in Figure 34. The single molecule SERRS collected with the regular 50x objective can also be seen at the bottom of Figure 34. The single molecule spectrum is reproducibly observed with three different optical set up.

4.3. Blinking Experiments and Results

One of the most interesting behaviours of single molecule spectroscopy is the on/off of the SERS signal "blinking" observed on some active silver or gold structures.[11,12,82-85]. The true origin of this behaviour is still under debate, recent research in several groups indicates that intermittent light emission could arise from long-lived triplet states in single dye molecules,[86] from efficient exciton traps in multichromophore system[87,88], from photogenerated quenching centers in CdSe nanocrystals[89] and from a slow temporal interruption of the electronic coupling between the adsorbed molecule and the metal particles.[83]. Our experiment data reveals that the intensity fluctuations of the SERRS signal from the LB samples containing 1,10 and 100 dye molecules were observed using 0.13 mW power of the 514.5 nm excitation line at room temperature as shown in Figure 34. For example, for the 100 molecules sample, statistical analysis for a total collection time of 1s and time interval of 1 second has shown that 28% of the collected spectral windows show the characteristic well defined spectrum given in Figure 35.

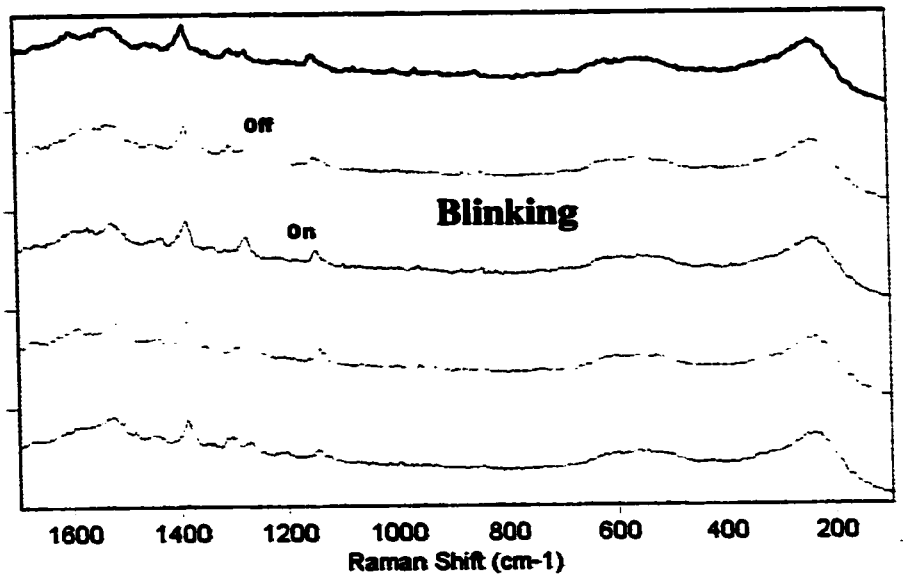

Figure 35 : The "On " and "Off" signal of single molecule. The spectra collected with 514.5 nm

CONCLUSION

The thesis presents a complete vibrational study of PTCD-NH_2 dye molecules using infrared and Raman techniques. Thin solid films of PTCD-NH_2 were fabricated using the LB technique and by sublimation. Reflection-absorption infrared spectroscopy was employed to determine the molecular orientation in the fabricated films. The molecular orientation of PTCD-NH_2 thin films evaporated onto Ag, extracted from RAIRS, is a tilted head-on orientation relative to the substrate.

Two methods of colloid preparation have been used to achieve SERRS of PTCD-NH_2. However, the single molecule SERRS spectra of PTCD-NH_2 were obtained only on colloidal silver particles prepared by citrate reduction. The properties of the single molecule SERRS are supported by SERRS spectra of LB-monolayers containing 1, 10 and 100 molecules per micron square coated with colloidal particles and a silver overlayer of 6 nm mass thickness. Overtone progressions are observed for the LB-SERRS on silver island films and silver colloid containing 10^{-7}M analyte up to the third overtone and combination of characteristic fundamentals. The first overtone and combinations are also observed in the single molecule spectrum providing ultimate assignment for the observed Raman bands. The ability to detect a single molecule in an LB-monolayer, and on colloidal silver, is dependent upon a number of instrumental parameters and experimental methods. Many elaborate methods are proposed to improve the experimental and collection efficiency for SMD.[83,90] or induce aggregation of the colloidal silver. In single molecule SERRS spectra of PTCD-NH_2 obtained here, there was no attempt to aggregate the colloidal silver prepared by citrate reduction method. The properties of the single molecule SERRS are reported for LB-monolayers containing 1, 10 and 100 molecules per micron square coated with colloidal particles and a silver overlayer of 6 nm mass thickness.

APPENDIX A

Synthesis: perylene-3,4,9,10-tetracarboxylic acid monoanhydride mono-n-butylimide

A stirred suspension of perylene-3,4,9,10-tetracarboxylic acid monoanhydride mono-n-butylimide (15.7 g, 0.040 mol) in 600 mL of toluene was treated with ethylene diamine (26.7 mL, 0.40 mole). The mixture was heated at reflux for 3 h then was cooled to room temperature and filtered. The solid was washed with 2 X 50 mL portions of toluene then was dried at 60°C. The crude product (19.15 g) was stirred in 500 mL of refluxing glacial acetic acid for 10 min and the hot suspension was filtered and the solid was washed with 2 X 50 mL of boiling acetic acid. The dried solid (5.02 g) was identified by ^{1}H NMR as the dimer formed from condensation of two moles of monoanhydride with one molecule ofethylenediamine . The filtrate was cooled to room temperature then was diluted, with vigorous stirring with 500 mL of isopropyl alcohol. Filtration, washing with isopropyl alcohol (2 x 100 mL) and drying gave the title product as dark brown solid (14.52 g, 66%). ^{1}H NMR: (300 mHz, 3:1 $CDCl_3$/TFA-d, internal TMS) 8.8 (two AB systems, 8H, perylene protons), 4.68 (broad t, 2H, imide N-C$\underline{H_2}$CH$_2$-NH$_3$+), 4.24 (t, 2H, imide N-C$\underline{H_2}$CH$_2$CH$_2$CH$_3$), 3.67 (broad t, 2H, -C$\underline{H_2}$NH$_3$+), 2.16 (s, 3H, C$\underline{H_3}$CO$_2$H), 1.76 (m, 2H, CH$_2$C$\underline{H_2}$CH$_2$CH$_3$), 1.49 (m,2H, CH$_2$CH$_2$C$\underline{H_2}$CH$_3$), 1.01 (t, 3H, CH$_2$CH$_2$CH$_2$C$\underline{H_3}$).

LIST OF PUBLICATION

- Tibebe Lemma, Ricardo, Aroca: Single molecule detection with surface-enhanced resonance Raman scattering on colloidal silver and silver island films. *Journal of Raman Spectroscopy*, 2002, 33,197-201.
- C. J. L. Constantino, T.Lemma, P.A. Antunes, R. Aroca: Single Molecule detection of a perylene dye dispersed in a Langmuir-Blodgett fatty acid monolayer using surface-enhanced resonance Raman scattering. *Spectrochimica Acta A*, 2002, 58, 403-409.
- Carlos J. L. Constantinao, Tibebe Lemma, Patricia A. Antunes, and Ricardo Aroca: Single molecule detection using surface enhanced resonance Raman scattering and Langmuir-Blodgett monolayer. *Analytical Chemistry*, 2001, 73, 3674-3678.

- R. Aroca, M. Nazri, T. Lemma , A. Rougier, GA. Nazri: Raman Spectra of Anode and Cathode Materials. NATO Sci. Ser., 385 (2000) 327-339

CONFERENCES and PRESENTATIONS

- **Tibebe Lemma**, Ricardo, Aroca, " Single molecule detection with surface- enhanced resonance Raman scattering on colloidal silver and silver island films" FACSS 2001, Detroit, Michigan, United State, October 2001.

- C. J. L. Constantino, S. Hadi, D. Ross , **T. Lemma** and R. Aroca, "Surface- Enhanced Absorption and Surface Enhanced Flourescence on Silver, Copper and Gold Island Films"84th CSC Conference and Exhibition. Montreal 2001. Montreal, Canada, May 2001.

POSTERS.

- C. J. L. Constantinao, **T. Lemma**, P. A. Antunes, and R. Aroca, " Spatially Resolved Single Molecule Detection of a Dye Dispersed in a Langmuir-Blodgett Monolayer Using Surface-Enhanced Resonance Raman Scattering" 84th CSC Conference and Exhibition. Montreal 2001. Montreal, Canada, May 2001.

REFERENCES

(1) Wilson, J. E. B.; Decius, P. C. C. *Molecular Vibrations; Theory of Infrared and Raman Vibrational Spectra.*; McGraw-Hill: New York, 1955.

(2) Bolkenshtein, M. B.; Gribov, L. A.; Eliasshevich, M. A.; Stepanov, B. I. *Molecular Vibrations* Nauka, Moscow, 1972.

(3) Woodward, L. A. *Introduction To The Theory Of Molecular Vibrational And Vibrational Spectroscopy.*; Oxford University Press, 1972.

(4) Chang, R. K.; Furtak, T. E. *Surface Enhanced Raman Scattering*; Plenum: New York, 1982.

(5) Kerker, M. *Selected Papers on Surface-enhanced Raman Scattering, SPIE Milestone Series.* Bellingham, 1990; Vol. MS 10.

(6) Kneipp, K.; Wang, Y.; Kneipp, H.; T. Perelman, L. T.; Itzkan, I. *Physical Review Letters* **1997**, *78*, 1667-1670.

(7) Nie, S.; Emory, S. R. *Science* **1997**, *275*, 1102-1106.

(8) Kneipp, K.; Kneipp, H.; Manoharan, R.; Itzkan, I.; Dasari, R. R.; Feld, M. S. *Applied Spectroscopy* **1998**, *52*, 175-178.

(9) Kneipp, K.; Kneipp, H.; V. Bhaskaran, K.; Ramasamy, M.; Geurt, D.; Irving, I.; Ramachandra R, D.; Michael S, F. *Physical Review E* **1998**, *57*, R6281-R6284.

(10) Kneipp, K.; Kneipp, H.; Itzkan, I.; Dasari, R. R.; Feld, M. S. *Chemical Reviews* **1999**, *99*, 2957-.

(11) Xu, H. X.; Bjerneld, E. J.; Kall, M.; Borjesson, L. *Physical Review Letters* **1999**, *83*, 4357-4360.

(12) Michaels, A. M.; Nirmal, M.; Brus, L. E. *J. Am. Chem. Soc.* **1999**, *121*, 9932-9939.

(13) Constantino, C. J. L.; Lemma, T.; Antunes, P. A.; Aroca, R. *Anal. Chem.* **2001**, *73*, 3674-3678.

(14) Michaels, A. M.; Jiang, J.; Brus, L. E. *J. Phys. Chem. B* **2000**, *14*, 11965-11971.

(15) Kneipp, K.; Kneipp, H.; Manoharan, R.; Itzkan, I.; Dasari, R. R.; Feld, M. S. *Journal of Raman Spectroscopy* **1998**, *29*, 743-747.

(16) Kneipp, K.; Kneipp, H.; Kartha, V. B.; Manoharan, R.; Deinum, G.; Itzkan, I.; Dasari, R. R.; Feld, M. S. *Physical Review E* **1998**, *57*, R6281-R6284.

(17) Krug II, J. T.; Wang, G. D.; Emory, S. R.; Nie, S. *J. Am. Chem. Soc* **1999**, *121*, 9208.

(18) Kneipp, K.; Wang, Y.; Kneipp, H.; Perelman, L. T.; Itzkan, I.; Dasari, R. R.; Feld, M. S. *Physical Review Letters* **1996**, *76*, 2444.

(19) Kneipp, K.; Kneipp, H.; Itzkan, I.; Dasari, R. R.; Feld, M. S. *Chemical Physics* **1999**, *247*, 155-162.

(20) Moskovits, M. *Reviews of Modern Physics* **1985**, *57*, 783-826.

(21) Kneipp, K.; Wang, Y.; Kneipp, H.; Perelman, L. T.; Itzkan, I.; Dasari, R. R.; Feld, M. S. *Phys. Rev. Lett.* **1997**, *78*, 1667-1670.

(22) Azumi, T.; McGlynn, S. P. *J. Chem. Phys.* **1965**, *42*, 1675.

(23) Kneipp, K.; Kneipp, H.; Manoharan, R.; Hanlon, E. B.; Itzkan, I.; Dasari, R. R.; Feld, M. S. *Applied Spectroscopy* **1998**, *52*, 1493-1497.

(24) Emory, R. S.; Haskins, W. E.; Nie, S. *J. Am. Chem. Soc* **1998**, *120*, 8009-8010.

(25) Fleishman, M.; Van Duyne, R. P.; McQuillan, A. J. *Chem. Phys. Lett.* **1974**, *26*, 163.

(26) Jeanmaire, D. L.; Van Duyne, R. P. *J. Electroana. Chem* **1977**, *84*, 1.

(27) Albrecht, M. G.; Creighton, J. A. *J. Am. Chem. Soc.* **1977**, *99*, 5215.

(28) Otto, A. *Light Scattering in Solids, Vol, IV, EDs. M. Cardona & G. Guntherodt.*, 1984.

(29) Birke, R. L.; Lombardi, J. R. *Spectrochemistry: Theory and Practice, Chapter 6 ,Surface-enhanced Raman scattering*; Plenum Press: New York, 1988.

(30) Creighton, J. A. *Spectroscopy of Surfaces, Chapter 2, The Selection Rules for Raman Spectroscopy*; John Wiley & Sons Inc.: Chichester, 1988.

(31) Pettinger, B. *In situ Raman Spectroscopy at metal Electrodes. Adsorption of Molecules at Metal electrodes*; VCH, 1988.

(32) Campion, A.; Kambhampati, P. *Chem. Soc. Rev* **1998**, *27*, 241.

(33) Vo-Dinh, T. *Trends in Analytical Chemistry* **1998**, *17*, 557-582.

(34) Aroca, R. F.; Kovacs, G. J. *Surface Enhanced Raman Spectroscopy in Vibrational Spectra and Structure.*; Elsevier: Amsterdam, 1991.

(35) Kambhampati, P.; Child, C. M.; Foster, M. C.; Campion, A. *J. Chem. Phys.* **1998**, *108*, 5013-5026.

(36) Weaver, G. C.; Zou, S.; Chan, H. Y. H. *Anal. Chem* **2000**, *72*, 38A-47A.

(37) Kneipp, K. *Experimentelle Technik der Physik* **1990**, *38*, 3-28.

(38) Tamarat, P.; Maali, A.; Lounis, B.; Orrit, M. *Journal of Physical Chemistry A* **2000**, *104*, 1-16.

(39) Constantino, C. J. L.; Lemma, T.; Antunes, P. A.; Aroca, R. *Spectrochimica Acta Part A* **2002**, *58*, 403-409.

(40) Baldwin, K. J.; Batchelder, D. N. *Applied Spectroscopy* **2001**, *55*, 517524.

(41) Wilson, T. *J. Microscopy* **1989**, *154*, 143.

(42) Frisch, M. J.; Trucks, G. W.; Schlegel, H. B.; Scuseria, G. E.; Robb, M. A.; Cheeseman, J. R.; Zakrzewski, V. G.; Montgomery. Jr, J. A.; Stratmann, R. E.; Burant, J. C.; Dapprich, S.; Millam, J. M.; Daniels, A. D.; Kudin, K. N.; Strain, M. C.; Farkas, O.; Tomasi, J.; Barone, V.; Cossi, M.; Cammi, R.; Mennucci, B.; Pomelli, C.; Adamo, C.; Clifford, S.; Ochterski, J.; Petersson, G. A.; Ayala, P. Y.; Cui, Q.; Morokuma, K.; Malick, D. K.; Rabuck, A. D.; Raghavachari, K.; Foresman, J. B.; Cioslowski, J.; Ortiz, J. V.; Stefanov, B. B.; Liu, G.; Liashenko, A.; Piskorz, P.; Komaromi, I.; Gomperts, R.; Martin, R. L.; Fox, D. J.; Keith, T.; Al-Laham, M. A.; Peng, C. Y.; Nanayakkara, A.; Gonzalez, C.; Challacombe, M.; Gill, P. M. W.; Johnson, B.; Chen, W.; Wong, M. W.; Andres, J. L.; Gonzalez, C.; Head-Gordon, M.; Replogle, E. S.; Po, J. A.; Gaussian, Inc: Pittsburgh PA, 1998.

(43) Nagata, Y.; Watanabe, Y.; Fujita, S.; Dohmaru, T.; Taniguchi, S. *J. Chem. Soc. Commun* **1992**, *21*, 1620.

(44) Henglein, A.; Mulvaney, P.; Linnert, T.; Holtzwarth, A. *J. Phys. Chem.* **1992**, *96*, 2411.

(45) Neil, S.; Ulrich, N.; Siegfried, S. *Journal of Colloid and Interface Science* **1999**, *211*, 122-129.

(46) Lee, P. C.; Meisel, D. D. *Phys. Chem* **1982**, *86*, 3391-3395.

(47) Emory, S. R.; Nie, S. *Book of Abstracts, 213th ACS National Meeting, San Francisco, April 13-17* **1997**, PHYS-459.

(48) Emory, S.; Nie, S. *J. Phys. Chem. B* **1998**, *102*, 493.

(49) Creighton, J. A.; Blatchford, C.; Albrecht, M. G. *J. Chem. Soc. Faraday Trans* **1979**, *75*, 790.

(50) Schneider, S.; Halbig, P.; Grau, H.; Nickel, U. *Photochem. Photobiol.* **1994**, *60*, 605.

(51) Ambrose, W. P.; Basche, T. H.; Moerner, W. E. *J. Chem. Phys.* **1991**, *95*, 7150-7163.

(52) Binnig, G.; Quate, C. F. *Physical Review Letters* **1986**, *56*, 930.

(53) Mercadante, R.; Tris, M.; Duff, J.; Aroca, R. *J. Mol. Struct. (Theochem)* **1997**, *394*, 215.

(54) Adachi, M.; Murata, Y.; Nakumura, S. *J. Phys. Chem.* **1995**, *99*, 14240.

(55) Rodriguez-Liorente, S.; Aroca, R.; Duff, J. *Spectrochimica Acta Part A* **1999**, *55*, 969.

(56) Kasha, M.; Rawls, H. R.; El-Bayoumi, M. A. *Pure Appl. Chem.* **1965**, *11*, 371.

(57) Hochstrasser, R. M.; Nyi, C. A. *J. Chem. Phys.* **1980**, *72*, 2591.

(58) Wokaun, A. *Mol. Phys.* **1985**, *56*, 1.

(59) Kummerlen, J.; Leiner, A.; Brunner, H.; Aussenegg, F. R.; Wokaun, A. *Mol. Phys.* **1993**, *80*, 1031.

(60) Cance, R. R.; Prock, A.; Silbey, R. *Adv. Chem. Phys.* **1978**, *37*, 1.

(61) Tanaka, J. *Bull. Chem. Soc. Jpn.* **1963**, *36*, 1237.

(62) Scott L, A. P.; Random, L. *J. Phys. Chem.* **1996**, *100*, 16502.

(63) Wong, M. W. *Chem. Phys. Lett.* **1996**, *256*, 391.

(64) Guhathakurta-Ghosh, U.; Aroca, R. F.; Nagao, Y. *Journal of Raman Spectroscopy* **1989**, *20*, 795-800.

(65) Rodriguez-Liorente, S.; Aroca, R.; Duff, J.; de Saja, J. A. *Thin Solid Films* **1998**, *317*, 129-132.

(66) Johnson, E.; Aroca, R.; Nagao, Y. *J. Phys. Chem.* **1991**, *95*, 8840-8843.

(67) Aroca, R.; Maiti, A. K.; Nagao, Y. *Journal of Raman spectroscopy* **1993**, *24*, 1993.

(68) Johnson, E.; Aroca, R. *Appl. Spectroscopy* **1995**, *49*, 472.

(69) Umemura, J.; Kamata, T.; Kawai, T.; Takenaka, T. *J Phys. Chem* **1990**, *94*, 62.

(70) Halls, M. D.; Schlegal, H. B. *Journal of Chemical Physics* **1999**, *111*, 8819-8824.

(71) Aroca, R. F.; Constantino, C. J. L.; Duff, J. *Appl. Spectrosc.* **2000**, *54*, 1120-1125.

(72) Aroca, R. F.; Constantino, C. J. L. *Langmuir* **2000**, *16*, 5425-5429.

(73) Kam, A.; Aroca, R. *Journal of vibrational spectroscopy* **2000**, *4*, 6.

(74) Aroca, R. F.; Guhathakurta-Ghosh, U.; Loufty, R. O.; Nagao, Y. *Spectrochim. Acta, Part A* **1990**, 717-722.

(75) Aroca, R.; Corio, P.; Rubim, J. C. *Ann. Chim. (Rome)* **1997**, *87*, 1-7.

(76) Weitz, D. A.; Garoff, S.; Gerson, J. I.; Nitzan, A. *J. Chem. Phys.* **1983**, *78*, 5324.

(77) Pettinger, B.; Krischer, K. *J. Electron Spectrosc. Relat. Phenom.* **1987**, *45*, 133-142.

(78) Kim, W.; Safonov, V. P.; Shalaev, V. M.; Armstrong, R. L. *Physical Review Letters* **1999**, *82*, 4811-4814.

(79) Maxwell, D. J.; Emory, S. R.; Nie, S. *Chem. Mater.* **2001**, *13*, 1082-1088.

(80) Kam, A. P.; Aroca, R.; Duff, J.; Tripp, C. P. *Langmuir* **2000**, *16*, 1185-1188.

(81) Constantino, C. J. L.; Lemma, T.; Antunes, P. A.; Aroca, R. *Analytical Chemistry* **2001**, *73*, 3674-3678.

(82) Nie, S.; Emory, S. R. *Science (Washington, D. C.)* **1997**, *275*, 1102-1106.

(83) Doering, W. E.; Nie, S. In *J. Phys. Chem.B*, 2002; Vol. 106, pp 311-317.

(84) Bjerneld, E. J.; Johansson, P.; Kall, M. *Single Molecule.* **2000**, *1*, 239-248.

(85) Moyer, P. J.; Schmidt, J.; Eng, L. M.; Meixner, A. J.; Sandmann, G. W.; Dietz, H.; Plieth, W. *J. Am. Chem. Soc.* **2000**, *122*, 5409-5410.

(86) Ha, T.; Enderle, T.; Chemla, D. S.; Selvin, P. R.; Weiss, S. *Chem. Phys. Lett.* **1997**, *271*, 1-5.

(87) Vanden Bout, D. A.; Yip, W. T.; Hu, D.; Fu, D. K.; Swager, T. M.; Barbara, P. F. *Science* **1997**, *277*, 1074-1077.

(88) Wai-Tak, Y.; Dehong, H. *J. Phys. Chem. A* **1998**, *102*, 7564-7575.

(89) Nirmal, M.; Dabbousi, B. O.; Bawendi, M. G.; Macklin, J. J.; Trautman, J. K.; Harris, D. J.; Brus, L. E. *Nature* **1996**, *383*.

(90) Nie, S. *Abstr. Pap.- Am. Chem. Soc. (2001) 221st PHYS-110* **2001**.

VITA AUCTORIS

BIRTHDATE:	**September 28, 1969.**	**Harrar, Harraghe, Ethiopia**
EDUCATION:	**1993-1994**	**City Adult Learning Center Toronto, Ontario.**
	1994-1999	**University of Windsor Windsor, Ontario**
	2000-2002	**University of Windsor Windsor, Ontario**